Article

Covariation of hot spring geochemistry with microbial genomic diversity, function, and evolution

Daniel R. Colman [1] ✉, Lisa M. Keller[1], Emilia Arteaga-Pozo[2],
Eva Andrade-Barahona[2], Brian St. Clair[2], Anna Shoemaker [3], Alysia Cox [2] &
Eric S. Boyd [1] ✉

The geosphere and the microbial biosphere have co-evolved for ~3.8 Ga, with many lines of evidence suggesting a hydrothermal habitat for life's origin. However, the extent that contemporary thermophiles and their hydrothermal habitats reflect those that likely existed on early Earth remains unknown. To address this knowledge gap, 64 geochemical analytes were measured and 1022 metagenome-assembled-genomes (MAGs) were generated from 34 chemosynthetic high-temperature springs in Yellowstone National Park and analysed alongside 444 MAGs from 35 published metagenomes. We used these data to evaluate co-variation in MAG taxonomy, metabolism, and phylogeny as a function of hot spring geochemistry. We found that cohorts of MAGs and their functions are discretely distributed across pH gradients that reflect different geochemical provinces. Acidic or circumneutral/alkaline springs harbor MAGs that branched later and are enriched in sulfur- and arsenic-based O_2-dependent metabolic pathways that are inconsistent with early Earth conditions. In contrast, moderately acidic springs sourced by volcanic gas harbor earlier-branching MAGs that are enriched in anaerobic, gas-dependent metabolisms (e.g. H_2, CO_2, CH_4 metabolism) that have been hypothesized to support early microbial life. Our results provide insight into the influence of redox state in the eco-evolutionary feedbacks between thermophiles and their habitats and suggest moderately acidic springs as early Earth analogs.

The microbial biosphere and the geosphere (comprising the lithosphere, hydrosphere, cryosphere, and atmosphere) have changed in concert for ~3.8 Ga[1–3]. Subaerial hydrothermal systems (i.e. hot springs) are among the earliest known habitats to support microbial life, as evinced by ~3.5 Ga fossil and geochemical evidence of microorganisms and their activities preserved in ancient hot spring deposits[4,5]. Phylogenetic and inferred physiologic data also consistently place microbial thermophiles as among the earliest-branching lineages and suggest that they were supported by anaerobic, chemoautotrophic metabolisms

dependent on geogenic energy substrates[6,7]. Concomitantly, contemporary continental hydrothermal systems host diverse and abundant microbial communities[8–11], largely attributed to the extensive geochemical variation and abundant energy substrates available in these environments[8,9,12]. At the highest temperatures (>~74 °C in circumneutral springs and >~54 °C in acidic springs), photosynthetic metabolism is excluded in hot springs and microbial productivity is driven by chemoautotrophic metabolism supported by geogenic energy substrates like H_2S, H_2, CO_2, and S^0[13–16]. Consequently,

[1]Department of Microbiology and Cell Biology, Montana State University, Bozeman, MT, USA. [2]Department of Chemistry and Geochemistry, Montana Technological University, Butte, MT, USA. [3]Department of Earth Sciences, Montana State University, Bozeman, MT, USA.
✉e-mail: daniel.colman@montana.edu; eric.boyd@montana.edu

contemporary high-temperature springs and the communities they support provide an opportunity to understand how chemosynthetic populations were supported on early Earth and how they have evolved alongside their hydrothermal habitats over geologic time.

The extensive variation in the geochemical composition observed within hot springs is generated by a convergence of several surface and subsurface processes. In most systems, oxic meteoric or saline waters infiltrate the crust and are heated to high temperature, forming a hydrothermal aquifer[17,18]. These hydrothermal aquifer fluids tend to be solute rich (e.g. of Na^+ and Cl^-) due to extensive high-temperature water-rock reactions and are infused with magmatic gases like CO_2, ^3He, and SO_2, the latter of which disproportionates at high temperature in the presence of water to form SO_4^{2-} and H_2S or S^0, depending on temperature and sulfur concentrations[19]. During circulation in the subsurface and their ascent to the surface, hydrothermal fluids become depleted in oxygen and are further enriched in crustal or meteoric gases such as CH_4, ^4He, and H_2[17,18,20,21]. The development of stark chemical variation in waters principally arises from fluids undergoing decompressional boiling during their ascent along fractures and faults, resulting in separation of fluids into a lower-density vapor phase carrying volatile gases (e.g. CO_2, H_2S, H_2, and CH_4) and a higher density liquid phase comprising non-volatilizing solutes (e.g. Na^+ and Cl^-)[17,18,22]. The low-density vapor phase can continue ascending to the surface and form fumaroles or otherwise condense with near-surface waters[18,23]. Condensation of vapor phase gases with near surface fluids equilibrated with atmospheric O_2 can result in the oxidation of H_2S, resulting in the formation of S^0 and ultimately sulfuric acid (H_2SO_4)[23–25]. The oxidation of H_2S and S^0 compounds is likely driven, at least in part, by O_2-dependent thermoacidophilic Archaea[25–29] that may have diverged from neutrophilic ancestors over only the past ~1 Ga[28]. The separation of fluids into a vapor phase and a liquid phase and subsequent oxidation of H_2S to form SO_4^{2-} and acid leads to the bimodal distribution of hot spring pH observed globally[30]. This includes the two primary types of hot springs in contemporary geothermal fields: acid-sulfate and circumneutral-alkaline springs. Given that O_2 only began to accumulate in the atmosphere ~2.4 Ga and only reached present-day levels at ~0.8 to 0.6 Ga (as summarized in ref. 31), acidic hot springs and the thermoacidophiles they host are likely to be relatively recent phenomena on Earth[28].

Circumneutral to alkaline pH hot springs are the surface expression of the liquid phase and thus tend to be gas- and oxidant-poor, the latter of which is due to long residence times in the subsurface[22] that permit extensive water-rock reactions and consumption of oxidants[17]. Paradoxically, these springs are often dominated by obligately aerobic bacteria within the Aquificales order[32–34] and have recently been argued to only be habitable due to the infusion of atmospheric O_2 once the waters reach the surface[22,35]. It is consequently unclear whether acidic hot springs or circumneutral/alkaline hot springs could have been prevalent microbial habitats on early Earth when O_2 was not readily available. Springs with pH intermittent to acid-sulfate and circumneutral/alkaline types are globally more rare[30] and occur due to dilution of hydrothermal water by meteoric water or by mixing of meteoric and/or hydrothermal water/gasses[36,37]. Thus, while hot spring ecosystems are often invoked as suitable analogs for investigating early life[4,38], it remains unclear how well their contemporary geochemistry and microbiology reflect early Earth conditions.

The most widely studied hydrothermal system is in Yellowstone National Park (YNP) that is host to >10,000 geothermal features that widely vary in their geochemical composition[12,17,24,25,39]. Extensive spatial geochemical variation among hot springs selects for unique assemblages of microorganisms with diverse functionalities[8,10,11,34]. However, the provenance of this taxonomic and functional diversity and their distributions remain unclear, in particular, given that the geochemical compositions of hydrothermal waters are likely to have substantively changed over Earth history as the Earth became more oxidized, as described above. Here, a census of hot spring genomic and functional diversity was generated alongside detailed geochemical measurements in 34 high-temperature hot springs (>61.9 °C) with conditions that preclude photosynthesis to evaluate the adaptive evolution of thermophilic lineages and their functions in coordination with their hydrothermal habitats. A total of 64 geochemical analytes were measured and 1022 metagenome-assembled-genomes (MAGs) were generated from community metagenomes from these springs. These data were also analyzed in conjunction with 444 MAGs generated from 35 metagenomes in our other recent studies[8,29,35,40–43].

Results

Geologic and geochemical context

Thirty-four sediment samples from 34 YNP springs with conditions that preclude photosynthesis (i.e. via a combination of pH, temperature, and sulfide[13,14]) were collected for metagenomic analysis (Supplementary Dataset 10). Water and dissolved gas samples were collected for geochemical analyses in coordination with sediment sampling (Supplementary Dataset 1). In addition, 35 previously published YNP hot spring samples (20 sediment samples and 15 water samples) from 19 other springs that were analyzed in our other studies (Supplementary Dataset 1) were included in the analyses and were similarly sampled and processed[8,35,40–43]. The 53 springs were located in 14 geothermal regions spanning a large geographic extent of YNP (Fig. 1a). The primary bedrock type in YNP is rhyolite (silica-rich, iron-poor rock) due to rhyolitic eruptions and lava flows from the Yellowstone caldera, although minor basalt flows (silica-poor, iron-rich rock) are present in discrete regions of YNP (Fig. 1a). The geyser basins sampled were primarily located in rhyolite formations[44,45] including in the Smokejumper (SJ), Middle Geyser Basin (MGB), Lower Geyser Basin (LGB), Upper Geyser Basin (UGB), Gibbon River (GRV), Sylvan Springs (SYL), Geyser Creek (GCR), Norris Geyser Basin (NOR), Norris-Mammoth Corridor (NMC), Seven Mile Hole (SMH), Crater Hills (CRH), Phantom Fumarole (PFU), and Greater Obsidian Pool Area (GOPA) (Fig. 1a). Geochemical analyses have indirectly suggested the interaction of thermal waters with sedimentary formations in the Washburn (WB) geyser basin[17] that is underlaid by the Absaroka Volcanic Supergroup formation that contains basaltic, andesitic (intermediate silica and iron), and dacitic (intermediate silica and iron) components[46]. Thus, the broad geologic context for most of the geyser basins sampled in this study was similar, except for the one spring from the WB area (Fig. 1a).

The range of spring pH (1.3–8.9) and temperature (61.9–92.8 °C) among the 69 total samples encompassed previously documented ranges of YNP springs that host non-photosynthetic communities (Fig. 1b)[13,14,47]. In addition, the spring waters exhibited variation in geochemistry spanning that previously observed for YNP springs (Fig. 1c)[25]. Sulfate (SO_4^{2-}) and chloride (Cl^-) concentrations are often used to identify the sources of fluids to hot springs globally[18,25]. Dilute meteoric-only (MO) waters are sourced from near surface aquifers that are recharged with recent snowmelt or rainfall and carry little solute content, including low concentrations of SO_4^{2-} or Cl^-[25] (Fig. 1c). The infusion of vapor phase gas containing sulfide into meteoric waters (meteoric water + gas, MG) leads to acidic waters with elevated SO_4^{2-} concentrations, but minimal Cl^- concentrations (Fig. 1c)[25]. The deep hydrothermal aquifer of YNP is estimated to have residence time estimated as between ~300 and ~1500 years[22], although earlier estimates suggested ages of >10,000 years[48] and its waters have high Cl^- concentrations due to more extensive high-temperature water-rock interactions in the subsurface[17]. Springs sourced by the deep hydrothermal aquifer, or those termed hydrothermal only (HO), therefore have elevated Cl^- and moderate SO_4^{2-} concentrations, the latter being derived from the initial disproportionation of SO_2[25]. Mixing of the aforementioned water types can result in waters intermediate to the end-member compositions described above, while additional infusion of gas (e.g. H_2S) and boiling can lead
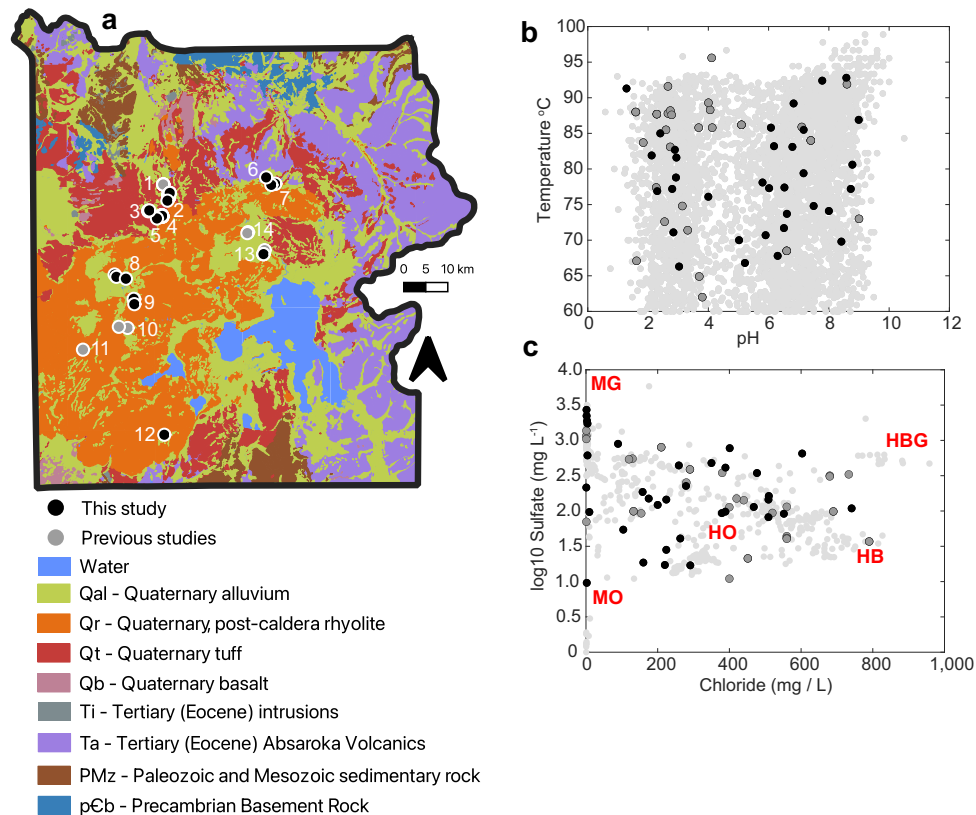
Fig. 1 | Locations of 69 Yellowstone National Park (YNP) hot spring samples analyzed in this study and major geochemical parameters measured in spring waters. a Map of sampling locations within YNP, modified from USGS I-711, as indicated in the Materials and Methods. Hydrothermal regions are labeled as follows: 1: Norris-Mammoth Corridor (NMC), 2: Norris Geyser Basin (NOR), 3: Sylvan Springs (SYL), 4: Geyser Creek (GCR), 5: Gibbon River (GRV), 6: Washburn (WB), 7: Seven Mile Hole (SMH), 8: Lower Geyser Basin (LGB), 9: Middle Geyser Basin (MGB), 10: Upper Geyser Basin (UGB), 11: Smokejumper (SJ), 12: Phantom Fumarole (PFU), 13: Greater Obsidian Pool Area (GOPA), 14: Crater Hills (CRH). The regions hosting the 34 springs newly analyzed here are indicated in black circles and those only hosting the springs from previous studies are shown in grey circles. **b** Spring pH and temperature of the 34 hot spring samples newly analyzed in this study (black circles) and the 35 from previous studies (dark grey circles) in context of 7706 measurements of YNP hydrothermal features from a previous geothermal survey (light grey circles; http://rcn.montana.edu). **c** The sulfate (SO$_4^{2-}$) and chloride (Cl$^-$) concentrations of the 34 hot spring samples newly analyzed in this study (black circles) and the 35 from previous studies (dark grey circles) in context of 488 other YNP hydrothermal features from a previous survey of YNP hot springs (as described in ref. 21). Five hot spring geochemical end-members (i.e. types) are indicated by text, as previously defined by Nordstrom et al. [25] and outlined in the text. MO meteoric only; HO hydrothermal only; MG meteoric + gas; HB hydrothermal only + boiling; HBG hydrothermal only + boiling + gas. The geographic coordinates and geochemical information for each site are provided in Supplementary Dataset 1.

to boiled hydrothermal-only waters (HB type) with greater solute-concentrations (Fig. 1c) or boiled hydrothermal waters with additional gas input (i.e. HBG type) type waters[25].

Using the above framework, representatives of nearly all hydrothermal water types previously documented in YNP were sampled (Fig. 1c), with the exception of HBG-type waters that comprise only a few known examples within YNP[25] and carbonate-rich waters in the Mammoth Hot Springs area that are also anomalous within YNP[17]. The springs were largely reflective of the bimodal pH observed in continental hot springs, with acid-sulfate springs (pH < ~5) and circumneutral alkaline-chloride springs (pH > ~7) representing the two most prevalent spring types[18,30]. In addition, several springs were sampled that were moderately acidic (e.g. pH ~ 5–7) that derived from mixing of different fluids, dilution of hydrothermal fluids with meteoric water, or infusion of meteoric waters with volcanic gas[25,42,49]. Consequently, these hot spring pH provinces (pH < 5, 5–7, and >7) were used to structure the subsequent analyses of geochemical and microbial biodiversity and are referred to as acidic springs (AS), mixed springs (MS), and circumneutral/alkaline springs (CS) henceforth.

Geochemical variation

The distributions of sample temperatures among the three pH groups were similar, owing to the strategy to sample as evenly as

possible across temperature and pH realms in springs that do not support photosynthesis (Supplementary Fig. 1). Likewise, water conductivity was similar among groups, except for some of the lowest conductivity values observed in MS springs (Fig. 2a), reflective of waters that arise when vapor phase gas mixes with dilute meteoric water[21] or when HO is diluted by meteoric water[50]. Nearly all waters were hypoxic (defined as those with <60 μM O$_2$ or ~0.95 mg/L[51] (Fig. 2b), with many also being suboxic (<~5 μM O$_2$ or ~0.16 mg/L) (Supplementary Dataset 1). This is consistent with the inverse exponential relationship between O$_2$ solubility and temperature[12]. MS geochemistry (pH 5–7) reflected values intermediate to many of those measured in AS and CS, including of SO$_4^{2-}$ (Fig. 2c; expected to be highest in AS, as discussed above); Cl$^-$ (Fig. 2d; expected to be highest in CS, as discussed above), metals like Fe(II) or total Fe (Fig. 2i; Supplementary Figs. 1–4), dissolved organic carbon (DOC), Fig. 2k and dissolved inorganic carbon (DIC) (Supplementary Fig. 1). Concentrations of gases (H$_2$, CH$_4$, and CO$_2$; Fig. 2e–g), in addition to total dissolved sulfide (Fig. 2h), were equivalent or higher among MS than AS (only CO$_2$ was significantly higher), possibly due to increased contributions of gas input to some MS[21,42] and the formation of some AS by additional vapor phase gas input. Further, some metals exhibited higher concentrations in MS or CS that could be related to sourcing by deeper circumneutral/
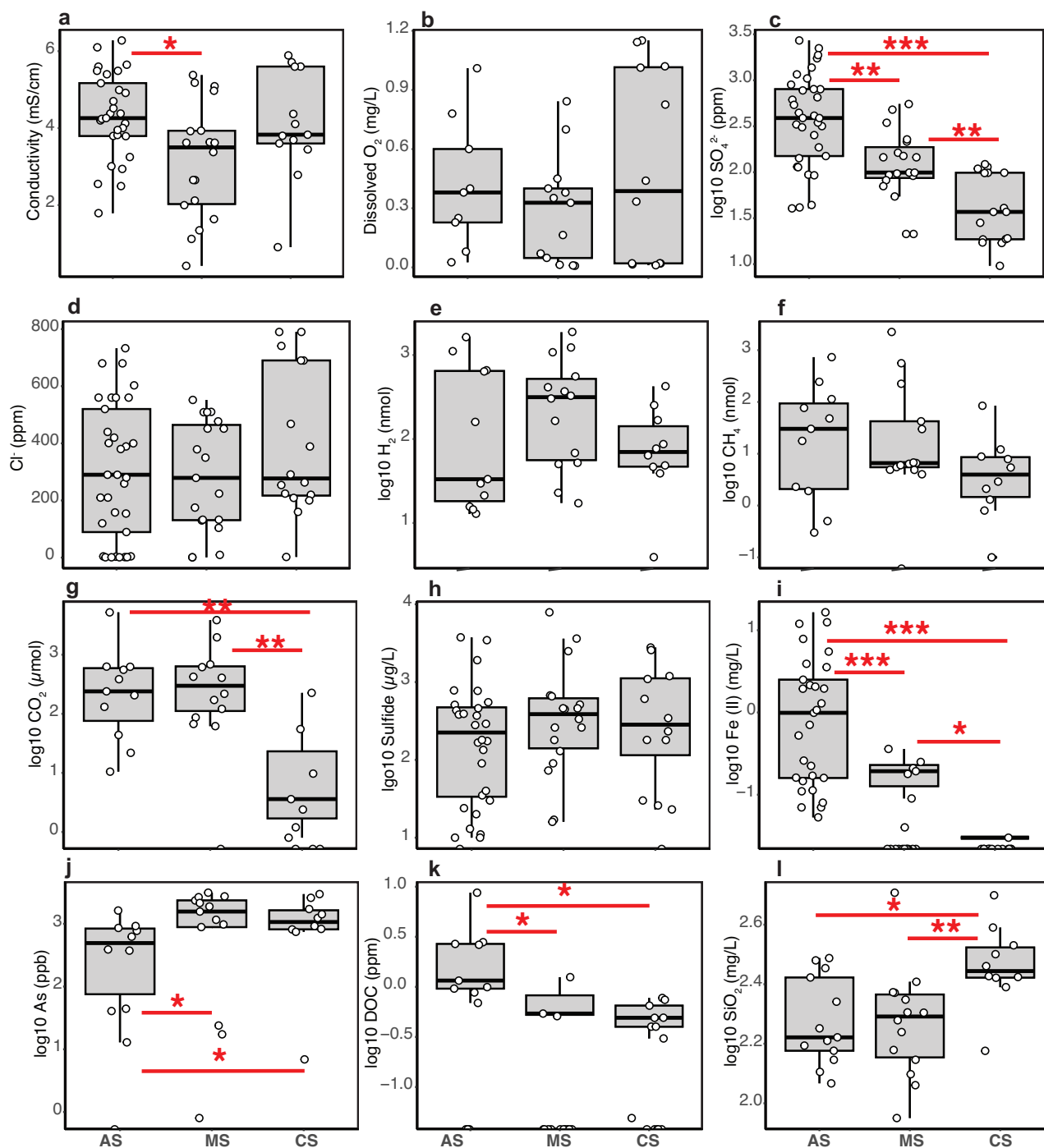
Fig. 2 | Variation in select geochemical parameters measured in 69 Yellowstone National Park (YNP) hot springs. Springs are organized as acidic (AS; pH < 5), mixed (MS; pH 5–7), and circumneutral/alkaline (CS; pH > 7) spring types. Boxplots for each parameter show the interquartile ranges of distributions in the grey boxes, with medians shown as black lines in the center of the boxes. Whiskers show the full ranges of the distributions. White circles show individual sample points and those beyond the whiskers are considered outliers. **a** Conductivity (n = 60), (**b**) dissolved oxygen (O_2) (n = 34), (**c**) sulfate (SO_4^{2-}, n = 68), (**d**) chloride (Cl^-; n = 68), (**e**) dissolved hydrogen (H_2) (n = 35), (**f**) dissolved methane (CH_4) (n = 35), (**g**) dissolved carbon dioxide (CO_2, n = 34), (**h**) total sulfide (n = 60), (**i**) ferrous iron (Fe(II), n = 61),

(**j**) total arsenic (As, n = 34), (**k**) dissolved organic carbon (n = 39), (**l**) dissolved silica (SiO_2, n = 37). Some parameters were log transformed when their ranges spanned several orders of magnitude. Statistical analysis in differences in distribution means was evaluated with pairwise Wilcoxon rank sum tests (with Benjamini & Hochberg correction for multiple comparisons), and statistically significant differences (two-sided) are shown between groups with red lines and asterisks: *: $p < 0.05$; **: $p < 0.01$; ***: $p < 0.001$. Exact p-values are shown in the accompanying Source Data file. Geochemical data are provided in Supplementary Dataset 1 and additional distributions of other analytes are shown in Supplementary Figs. 1–4.

alkaline fluids that undergo high-temperature water-rock interactions with rhyolitic bedrock. For example, arsenic (As) (Fig. 2j) exhibited the highest concentrations in CS, consistent with its sourcing from high-temperature reaction with rhyolite bedrock[52,53].

In addition, major ion composition was largely similar across springs (Supplementary Figs. 1–2), reflective of their sourcing within similar bedrock types. Nearly all waters were depleted in oxidized nitrogen species (i.e. NO_3^-, Supplementary Fig. 1; NO_2^- was below detection in
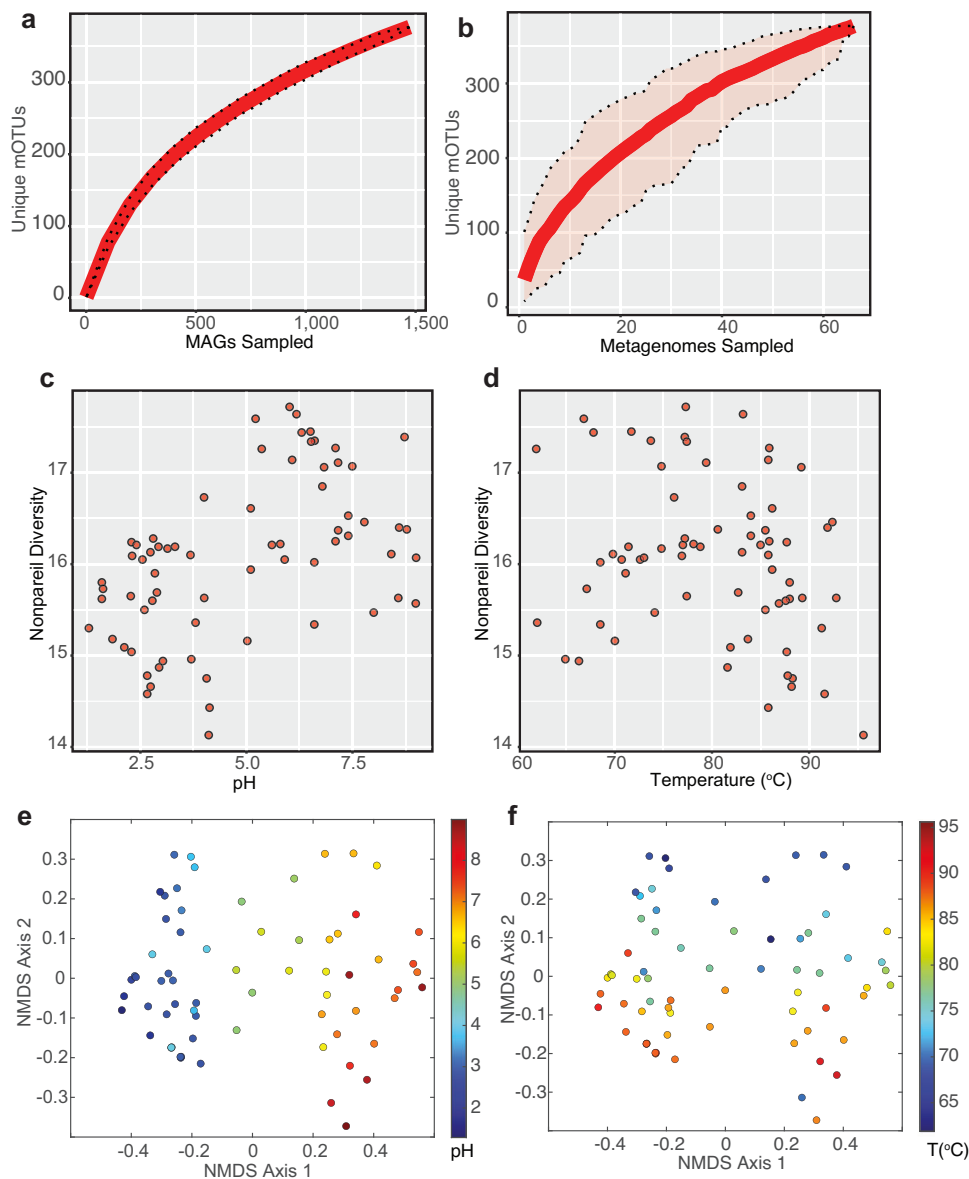
Fig. 3 | Genomic biodiversity present among 1466 metagenome-assembled-genomes (MAGs) recovered in this study from 69 Yellowstone National Park (YNP) hot springs. The 1466 MAGs were clustered into 372 metagenomic operational taxonomic units (mOTUs) at the 95% average nucleotide identity (ANI) level that approximately corresponds to species-level thresholds. Rarefaction curves showing the sampling of unique mOTU diversity with increasing recovery of MAGs (**a**) or with additional sample inclusion (**b**). The light red shading shows the expected 95% confidence intervals (not identifiable in panel a because they are less than the thickness of the line). **c, d** The genomic diversity, as measured with the Nonpareil diversity metric, in each metagenome in relationship to hot spring pH (2nd order polynomial regression; adjusted $R^2 = 0.26$, $p = 1.594 \times 10^{-5}$, two-sided) (**c**) or temperature (linear regression $R^2 = 0.043$, $p = 0.05$, two-sided) (**d**). **e, f** Nonmetric multidimensional scaling (NMDS) ordinations of hot spring mOTU composition based on variation in mOTU abundances across the 67 hot springs used for MAG reconstruction (2 previously published metagenomes were not used to generate MAGs, as described in the 'Methods'). Each community is colored by corresponding hot spring pH (envfit correlation; $R^2 = 0.87$, $p \le 0.001$, two-sided, uncorrected for multiple comparisons) (**e**) or temperature ($R^2 = 0.50$, $p < 0.01$, two-sided, uncorrected for multiple comparisons) (**f**). NMDS stress was 0.10. The rarefaction and NMDS plot source data are provided in the accompanying Source Data file, while the diversity values are provided in Supplementary Dataset 1.

all waters) and phosphate (PO_4^{3-}; Supplementary Fig. 1), with all values < 1 mg/L, except for one AS (SYL01; PO_4^{3-} concentration of ~15.6 mg/L; Supplementary Dataset 1).

Geochemical controls on genomic diversity

The 69 metagenomic libraries analyzed here (including the 34 newly described in this study) comprised ~2.3 Tbp of paired-end read data (average of 114×10^6 reads/sample) and 7.4 Gbp of assembled data (Supplementary Dataset 1). A total of 1466 metagenome-assembled-genomes (MAGs) of at least medium to high quality (>50% estimated

completeness and <10% contamination) were compiled from 67 of the metagenomes. Only the raw reads from 2 of the metagenomes (Old Faithful Geyser and Spouter Geyser) were used for taxonomic analyses, given the inability to generate appropriate quality MAGs from these samples, as previously described[43]. The MAGs comprised 372 metagenomic operational taxonomic units (mOTUs) defined at 95% average nucleotide identity (ANI) that approximately reflects species-level clusters[54]. The overall census of hot spring diversity was relatively complete, as indicated by rarefaction analysis of mOTUs (Fig. 3a) and based on the contribution of each metagenomic sample to the overall

mOTU count (Fig. 3b). Thus, the present study represents a nearly complete census of the species-level genomic diversity in high-temperature YNP springs.

Among the 1466 MAGs, 986 were archaeal and 480 were bacterial, representing 11 and 36 archaeal and bacterial phylum-level groups, respectively, in addition to one bacterial MAG from SMH02 that could not be classified to a known bacterial phylum (Supplementary Fig. 5; Supplementary Dataset 2). Many archaeal and bacterial MAGs were not classifiable (i.e. genomic database representatives are not available) at lower taxonomic ranks (classes, orders, families, and genera) (Supplementary Fig. 5). The level of unclassified taxa far surpassed estimates of uncharacterized archaeal and bacterial genomic diversity that have been considered high in other ecosystems including in the Arctic Ocean and Baltic Sea[55,56], while also rivaling that of a recent analysis of global deep-sea hydrothermal vents[57]. Unclassified taxa were not evenly distributed among springs or spring types, with springs exhibiting pH ranges between pH 5 and 7 (i.e. MS-type springs) harboring most of the unclassified diversity (Supplementary Fig. 5). Unclassified genus-level diversity was highly correlated with overall spring genomic diversity (measured via the Nonpareil diversity metric; linear regression adjusted $R^2 = 0.40$, $p < 0.001$, two-sided), suggesting that the most biodiverse springs in YNP are MS and that these host the least studied taxa (i.e. a lack of representatives in genomic databases).

To evaluate whether the MAG-based dataset accurately represented community taxonomic composition, MAG taxonomic classifications and their associated relative abundances were compared against estimates from assembly-free read-based taxonomic analyses for the 34 metagenomes newly described here. The agreement of the two relative abundance estimates was exceptionally high (Supplementary Fig. 6; adjusted $R^2 = 0.94$, slope = 1.02, $p < 0.001$), indicating that the MAG-based dataset robustly represented the taxonomic diversity present in each metagenome. These results are consistent with the genomic coverage analyses described above that suggested nearly complete coverage of genomic diversity for all metagenomes. Taxonomic classifications identified in the read-based analyses, but not in the MAG-based analyses, were also evaluated to assess whether specific taxa were systematically not identified in the MAG-based analyses. None of the read-based classifications that were absent in the MAG-based dataset exhibited estimated relative abundances > ~3% and only two had estimated relative abundances of > 1% (Supplementary Dataset 3). Taken together, the results suggest that the vast majority of taxa, including essentially all higher relative abundance taxa (e.g. ~ >1%), in the spring community metagenomes were present within the MAG-based analyses and their relative abundance estimates were robust to different estimation methods. Undoubtedly, very low-abundance taxa specific to one or a few springs may not be represented in the dataset, but significantly greater sequencing depth than the ~50–100 Gbp dedicated to each sample would be needed to enable recovery of at least medium-quality MAGs. The comprehensive nature of the sequence dataset generated herein was further scrutinized by comparison to an earlier genomic survey of high-temperature non-photosynthetic hot spring communities in YNP that was conducted with low-throughput sequencing methods and that recovered ~30 MAGs comprising ~15 phylotypes from 14 springs[58]. A comparison of the taxonomic identities of the entire assemblies from the previous 14 springs ($n = 297$ classifications; 154 unique) against those for the 1022 MAG assemblies newly produced here ($n = 2235$; 465 unique) revealed that all 154 unique taxonomic affiliations of sequences from the previous study were recovered, in addition to an overall >3-fold increase of taxonomic classifications in the newly reported MAG assemblies of this study (Supplementary Dataset 4). Collectively, these results suggest a highly comprehensive survey of the genomic and taxonomic diversity present within high-temperature YNP springs and represent a significant advancement in our understanding of the microbial biodiversity in these systems.

Genomic diversity was not uniformly distributed among spring types, with diversity (based on the Nonpareil diversity metric) highly associated with pH. An initial Pearson correlation analysis indicated a highly significant association with Nonpareil diversity and pH ($R = 0.51$, $p < 1 \times 10^{-5}$), along with weaker correlations to several other parameters. Specifically, the Nonpareil diversity metric was also significantly correlated with spring temperature ($R = -0.25$, $p = 0.039$), conductivity ($R = -0.35$, $p = 0.007$), $\delta18O$ ($R = -0.48$, $p = 0.001$), δD ($R = -0.43$, $p = 0.003$), DIC ($R = 0.36$, $p = 0.021$), DOC ($R = -0.40$, $p = 0.015$), Al ($R = -0.40$, $p = 0.020$), Ti ($R = -0.37$, $p = 0.030$), Pb ($R = -0.38$, $p = 0.028$), Th ($R = -036$, $p = 0.035$), and CO_2 ($R = -0.41$, $p = 0.016$). Most of these other parameters related to diversity were themselves highly correlated to pH (Supplementary Fig. 7, Supplementary Dataset 5), as expected given the role of pH in modulating analyte solubility, speciation, and availability (including of metals: Fe(II), total Fe, Al, Ti, Sb, Ba, La, Ce, Nd, and W; and chemical species: DIC and DOC). The association of Nonpareil diversity and pH exhibited a slightly humped relationship (Fig. 3c) that was slightly better fit with a 2nd-order polynomial regression; adj. $R^2 = 0.26$, $p < 0.0001$, two-sided) than a linear model (adj. $R^2 = 0.23$, $p = 0.0117$, respectively, two-sided). Temperature was only weakly negatively associated with genomic diversity (Fig. 3d; Pearson $R = -0.25$, $p = 0.0039$; linear regression adj. $R^2 = 0.04$, $p = 0.05$, two-sided), contrasting with previously observed temperature-dependent diversity patterns based on 16S rRNA gene sequence analyses of hot springs[59–61]. This distinction could arise from the use of community genomic data to evaluate biodiversity rather than 16S rRNA gene diversity, as has been used previously, but is also likely influenced by springs of this study spanning ~35 °C since lower-temperature springs (i.e. those where photosynthesis is possible) were not considered.

Intriguingly, conductivity was also significantly and inversely correlated to Nonpareil diversity (Pearson $R = -0.35$, $p = 0.007$, two-sided; linear regression adj. $R^2 = 0.11$, $p < 0.01$, two-sided), although conductivity was not correlated with temperature or pH (Supplementary Fig. 7, Supplementary Dataset 5). The peak in genomic diversity in MS is consistent with recent analyses suggesting that moderately acidic hot springs that exhibit greater evidence for mixing of different fluid types generally exhibit higher diversity[8,42,61]. In many cases, MS exhibit very low conductivity due to the mixing of vapor phase fluids with meteoric waters, while concomitantly harboring exceptionally high taxonomic and functional diversity[8]. Thus, MS represent biodiversity hot spots in YNP, likely due to underlying geological, hydrological, and geochemical processes that can promote the generation and mixing of oxidized and reduced fluids that generate and maintain biodiversity in hydrothermal systems. Similar observations have been made in deep sea hydrothermal environments, wherein complex subsurface mixing and hydrogeological processes supported exceptionally diverse thermophilic communities[62]. These observations point to the convergence of subsurface and surface processes in generating and maintaining microbial diversity, such as in the MS identified herein.

Among the 66 analytes that were evaluated, water pH best-explained community compositions across springs, followed by temperature (Fig. 3e, f; envfit correlation; $R^2 = 0.87$, $p < 0.001$ and $R^2 = 0.50$, $p < 0.01$, two-sided, uncorrected for multiple comparisons, respectively). Several other analytes were significantly ($p < 0.05$) correlated with community composition to a lesser extent than pH or temperature (Supplementary Dataset 6). However, all but four of these analytes were significantly correlated to pH (Supplementary Fig. 7; Supplementary Dataset 5), for reasons discussed above. Likewise, of the 4 analytes not significantly associated with pH: Ga, CO_2, and elevation were significantly correlated to temperature while B was significantly associated with concentrations of major ions indicative of bulk differences in water chemistry (e.g. Cl^-), suggesting that it is a proxy for major differences in water compositions (e.g. as a proxy for

circumneutral/alkaline springs with high Cl⁻ concentrations) (Supplementary Fig. 7; Supplementary Dataset 5). Thus, at the system-wide scale, pH and temperature are the only parameters that significantly influence community composition. It is nevertheless worth noting that other individual parameters likely constrain finer-scale taxonomic or functional distributions within spring types, as discussed in the following sections. The dominant influence of pH in structuring high-temperature spring communities is consistent with previous taxonomic compositional analyses of hot springs based on 16S rRNA gene surveys in YNP and elsewhere[9,34,61,63–66], in addition to earlier metagenomic analysis of 20 YNP hot springs[58] and meta-analyses of functional gene distributions among YNP hot springs[67–69].

Notably, the single community from a non-rhyolite setting (WB-02 from Washburn Hot Springs) harbored MAGs almost entirely within mOTUs that were common in other acidic hot springs across YNP (Supplementary Dataset 7), suggesting that the influence of bedrock setting was not as important as overall geochemistry for structuring microbial communities. A recent analysis of 16S rRNA gene amplicon sequence variant (ASV) profiles across continental hot spring systems from different geologic, tectonic, and geographic settings (YNP, Iceland, and Japan) revealed similar taxonomic groups across all regions[61]. Notably, spring pH was the greatest predictor of within-system diversity distributions, but with evidence for subtle variation in geochemistry across geologic settings being highly associated with overall variation in communities. Specific comparisons of rhyolite-hosted communities from Iceland and YNP revealed starkly different ASV compositions, despite being from springs with similar geochemical profiles (i.e. with similar pH and temperature). Further, many of the ASVs, including abundant ASVs, were shared between regions, indicating that dispersal limitation alone could not account for the observed community differences in geographically distant springs hosted in the same bedrock type. Thus, complex influences from geologic settings, dispersal limitations, and localized geologic/hydrologic characteristics all likely influence observed biogeographic patterns of hot spring biodiversity at within-system and global scales.

The inclusion of 35 previously published metagenomes (Supplementary Dataset 1) permitted some insights into the stability of communities in hot springs over time and differentiation among hot spring phases (e.g. water vs. sediment communities). Three of the springs investigated here were sampled across years, including three sediment metagenomes from 'Figure 8' spring (2013, 2018, and 2019), 2 sediment metagenomes from Perpetual Spouter (2018 and 2019; in addition to a water community metagenome from 2018), and 2 sediment metagenomes from Cinder Pool (2018 and 2019), in addition to 6 water metagenomes from Cinder Pool (from 0, 9, and 15 m depths in 2016 and 2020) (Supplementary Fig. 8). The sediment metagenome compositions were nearly identical in all three cross-year comparisons, even though the geochemistry of Cinder Pool dramatically changed (acidified from pH ~4 to pH ~2.5) between 2018 and 2019[41], as did 'Figure 8' across the sampling periods (Supplementary Fig. 8). Likewise, the depth-resolved samples from Cinder Pool from 2016 and 2020 were all nearly identical, despite spanning the period of spring acidification. In addition, while metagenomes concomitantly collected from waters and sediments of 6 different springs were generally compositionally similar, notable differences were observed for some springs, including for Perpetual Spouter and GCR-JH (PS and JH, respectively, in Supplementary Fig. 9). Thus, while overarching geochemical determinants like pH and temperature control hot spring composition overall, other factors including historical effects through time (e.g. succession following seismic activity[70]) and finer-scale geochemical differences in waters and sediments likely also contribute to variation[35,42,63]. Additional studies of the taxonomic and functional composition across a variety of temporal scales and spatial scales within springs would provide useful insights for identifying additional community structuring processes.

The pH-dependent variation in community composition reflected discrete pH ranges of individual taxa that likely point to their respective ecological niches (Fig. 4; Supplementary Figs. 10 and 11). For example, AS were dominated by Archaea, including the orders Sulfolobales, Desulfurococcales, and Thermoproteales (Fig. 4). The only bacterial taxa identified in AS was the *Hydrogenobaculum* genus (Aquificota). In contrast, diverse archaeal and bacterial taxa were prevalent among MS, consistent with the above diversity analyses. Lastly, Archaea including Desulfurococcales, Thermoproteales, and Caldarchaeales, along with *Thermocrinis* (Aquificota) and Armatimonadota Bacteria were particularly dominant members of CS. While some taxonomic groups were only identified in discrete pH ranges (e.g. Sulfolobales, Korarchaeales, and Bathyarchaeia Archaea, in addition to Deinococcota Bacteria; Fig. 4), many other taxonomic groups were arrayed across broad pH ranges. For example, the 38 Desulfurococcales mOTUs (comprising 303 MAGs) and 18 Thermoproteales mOTUs (comprising 143 MAGs) exhibited highly differentiated pH distributions, with both containing specific groups only found in AS, MS, or CS (Supplementary Fig. 10). Likewise, the nine mOTUs classified as *Thermocrinis* (26 MAGs) exhibited distinct pH ranges in either MS or CS, while the three mOTUs classified as *Sulfurihydrogenibium* (10 MAGs) also exhibited distinct pH ranges (Supplementary Fig. 11). These observations suggest the widespread presence of taxa (at various phylogenetic ranks) that have evolved to inhabit discrete geochemical provinces, as reflected by spring pH.

Network analysis of the correlations in abundance of the 372 mOTUs among the 67 metagenomes used for MAG-based analyses revealed the presence of discrete clusters of taxa, arrayed by the pH of the springs that they inhabited (Supplementary Fig. 12). mOTUs derived from AS with mean spring pH distributions of pH < 4 exhibited completely non-overlapping sub-networks relative to those derived from MS/CS. Likewise, separate clusters within the sub-network of mOTUs from MS/CS coincided with differences in mean pH distribution ranges (Supplementary Fig. 12). Thus, the network analysis suggested the presence of discrete species-level unit (i.e. mOTU) cohorts in springs with similar pH. Taken together, these results suggest that the geologic, hydrologic, and geochemical processes leading to hot spring geochemical variation (as proxied by pH) result in discrete ecological provinces that host discrete cohorts of taxa, implying the presence of eco-evolutionary dynamics among and between lineages and their hot spring environments.

Functional distributions across hot spring geochemical provinces

To determine how metabolic potentials of the MAGs align with variation in geochemistry, metabolic reconstructions were performed for the 1,466 MAGs recovered in this study (Fig. 5). A comparison of the estimated abundances of functions encoded by the 1022 newly generated MAGs to those within their entire corresponding metagenomic assembly revealed a high level of concordance (Pearson's $R = 0.99$; linear model adj. $R^2 = 0.97$, $p = 0$, slope = 0.80; Supplementary Fig. 13). Likewise, the overall variation in functional potential profiles from MAGs and those derived from entire metagenome assemblies were essentially identical (Supplementary Fig. 14). Consequently, while some functions encoded in the metagenomes may not have been identified in MAGs, as expected, the comparisons above and the nearly complete census of taxonomic diversity in the unassembled read datasets (described above) suggest that the MAG-based estimations of community functional potentials were comprehensive. In addition, functional profiles for mOTUs were based on consensus evidence from the MAGs within that mOTU that derived from different samples. Thus, while this represents a conservative approach to defining functions, the leveraging of independently generated MAGs across multiple springs provides additional confidence in the functional assessments described herein.
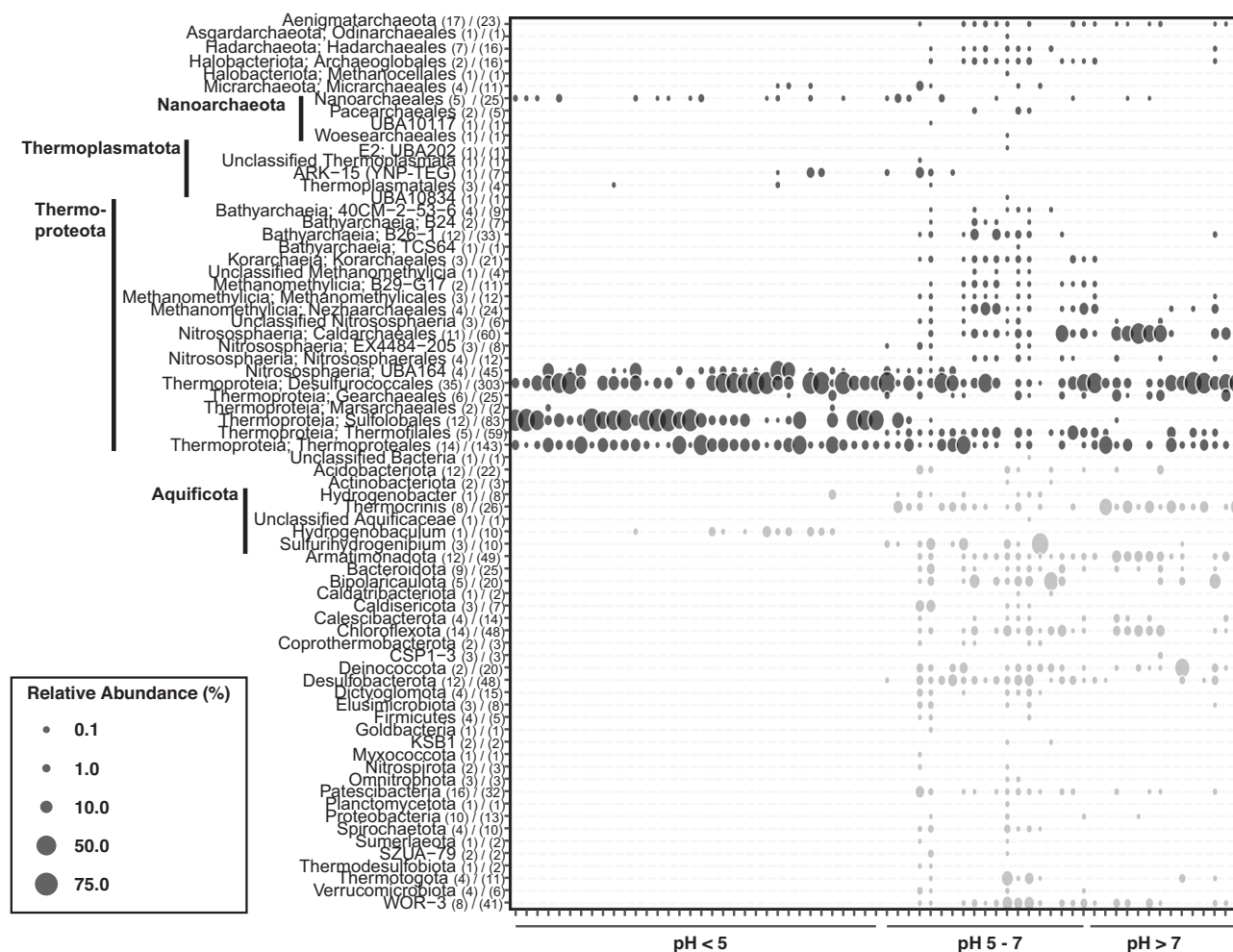
Fig. 4 | pH-dependent ecological distributions and evolutionary histories of hot spring taxa. Distribution of higher order taxonomic groups among 67 Yellowstone National Park (YNP) hot spring communities. Each column represents a single hot spring community metagenome, and each row represents a taxonomic group, identified on the left. The number of metagenomic operational taxonomic units (mOTUs) represented by each taxonomic classification is shown in parentheses, followed by the total number of MAGs within the mOTUs. Archaeal taxa are summed at the order level (phylum given before parentheses or shown to the left) while bacterial taxa are summed at the phylum level (except for the Aquificota that are shown as individual genera). Archaeal taxa are shown in black circles at the top while bacterial taxa are shown in lighter grey circles at the bottom. The estimated relative abundances are shown by circle size based on the scale in the bottom lower left. The estimated relative abundance values are provided alongside taxonomic and mOTU classification information in Supplementary Dataset 2.

Evaluation of the association of geochemistry with functional potential profiles encoded by members of communities (i.e. those related to energy metabolism) indicated that spring pH was again the strongest correlate to variation (envfit $R^2 = 0.61$; $p < 0.001$, two-sided, uncorrected for multiple comparisons; Supplementary Fig. 15). This is consistent with observations for the MAG distribution analyses (Fig. 3e) and also with our previous meta-analysis of functional genes among hot spring metagenomes[67]. Notably, temperature was not correlated to variation in MAG functional potential (envfit $R^2 = 0.01$; $p = 0.822$, two-sided, uncorrected for multiple comparisons). These results suggest a close relationship between taxonomic and metabolic diversification in association with hot spring geochemical variation and change. To evaluate the concordance of specific metabolic functions with hot spring geochemical provinces, the relative abundances of individual functions (i.e. those shown in Fig. 5) among the three spring types were evaluated and summarized by metabolic category below.

Carbon fixation and 1-carbon metabolism
The prevalence of C-fixation pathways significantly varied across spring type, largely due to the predominant taxa within the springs (Fig. 5, Supplementary Fig. 16). Specifically, the reverse TCA (rTCA)

C-fixation pathway was significantly more enriched in MS and CS type communities (Fig. 5, Supplementary Fig. 16) and was primarily attributed to Aquificota genera (*Thermocrinis*, *Sulfurihydrogenibium*, and *Hydrogenobacter*) in MS and CS (albeit through two pathway variants[33]) (Supplementary Dataset 8). The Aquificota have been inferred to be important primary producers in hot springs and exhibit taxon-specific, pH-dependent distributions[33,34], consistent with their distributions reported here (Fig. 4, Supplementary Fig. 11). While the Aquificota genus *Hydrogenobaculum* also encodes the rTCA pathway[33] (Supplementary Dataset 8) and were present in some AS in this study, they generally only comprised small proportions of their communities and are thus not likely major autotrophs across the AS springs examined herein (Supplementary Fig. 16; Supplementary Dataset 8). Ribulose-bisphosphate carboxylase (RuBisCO)-based (i.e. Calvin Cycle) carbon fixation was also statistically enriched in MS and CS, albeit only in relatively low abundance taxa, including *Thermus* and *Meiothermus* (family Thermaceae) and others (Supplementary Dataset 8, Supplementary Fig. 16). The potential for autotrophic or mixotrophic metabolism in Thermaceae remains enigmatic given prior identification of the potential for the Calvin Cycle in some isolates[71] although they are generally considered heterotrophic[72]. Nevertheless, some mixotrophic isolates have been reported from Iceland[73], so it is possible that
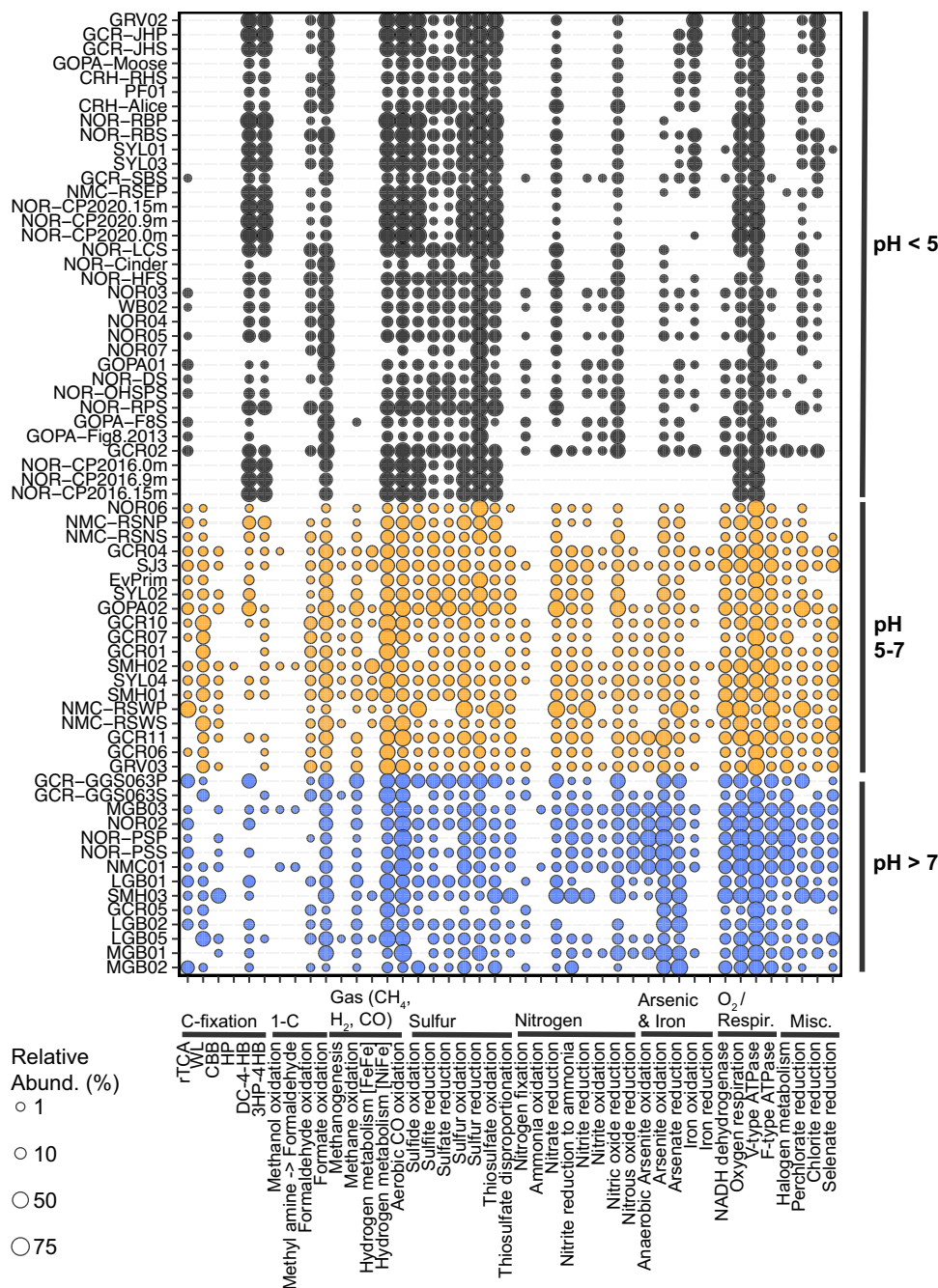
Fig. 5 | Functional potential of metagenome-assembled-genomes (MAGs) recovered from 67 hot spring community metagenomes. Metagenomes are arranged in order of increasing pH, as indicated to the right of the plot. Each predicted function is indicated by a column and is arrayed according to functional category as indicated below the plot. The circle sizes represent the summed relative abundances for all MAGs predicted to encode the given function for a given metagenome, with relative abundance values scaled to the legend on the bottom left. Distributions of the relative abundances for each specific function are individually shown in Supplementary Figs. 16, 17 and 19, 20, and the relative abundance estimations alongside functional inferences are provided in Supplementary Dataset 8.

Thermaceae may contribute to primary production via mixotrophic activity in MS and especially CS systems where they are ubiquitous.

The 3-hydroxypropionate/4-hydroxybutyrate (3-HP/4-HB) carbon fixation pathway typical of Sulfolobales[74] was only statistically enriched in AS springs and accordingly was primarily associated with Sulfolobales that were very abundant in those springs (Fig. 5; Supplementary Fig. 16; Supplementary Dataset 8). The dicarboxylate/4-hydroxybutyrate (DC/4-HB) carbon fixation pathway shares most of the enzymatic steps as the 3-HP/4-HB pathway[75] and was consequently considered present where the 3-HP/4-HB pathway was present, explaining its statistical enrichment among AS communities (Supplementary Fig. 16). In contrast to the above carbon fixation pathways, the

Wood-Ljungdahl (WL) pathway was statistically enriched in MS MAGs (Fig. 5, Supplementary Fig. 16) and was encoded by diverse archaeal and bacterial taxa (Supplementary Dataset 8). In addition to the consistent identification of WL pathways in recently characterized lineages (Supplementary Dataset 8), taxa not previously known to encode the WL pathway were identified, including two Caldarchaeales (formerly Aigarchaeota) mOTUs not classifiable to a known family (mOTU106 and mOTU235) and a Thermoplasmatota (Thermoplasmata) mOTU in an unclassified family (mOTU306). The widespread prevalence of the WL pathway suggests that it may be a broadly important autotrophic mechanism in MS-type communities. In addition, the distribution of the WL pathway among many members of MS communities (rather

than by a few dominant taxa) suggests that they may be ecologically structured more evenly than in AS and CS that were generally dominated by one or a few autotrophic populations. These results are consistent with a previous metagenomic study of Obsidian Pool (an MS type spring also sampled in this study as GOPA-01) that revealed enrichment of Archaea encoding the WL pathway[76]. The WL pathway is generally considered to be strictly associated with anaerobic Archaea and Bacteria (e.g. in methanogens, acetogens, and sulfate reducers)[77], in contrast to the rTCA and 3-HP/4-HB pathways of the generally aerobic Aquificota and Sulfolobales, respectively. Thus, the differential statistical enrichment of these three pathways among spring types suggests that the modes of primary productivity are related to the redox state of springs. Consistently, DO was generally lowest (but not statistically significantly lower) in MS springs (Fig. 2b). However, it should be noted that DO was only measured in 32 of the springs newly analyzed in this study in addition to one other previously published spring (Supplementary Dataset 1). Lastly, the 3-hydroxypropionate pathway was only identified in 2 low-abundance MAGs and is therefore not discussed further here.

Among the 1-carbon metabolisms evaluated here, formate oxidation capacity via formate dehydrogenases and formaldehyde oxidation (that involves some of the same genes as formate oxidation) was widespread among taxa and spring types, although formate oxidation was particularly statistically enriched in AS (Fig. 5; Supplementary Fig. 16; Supplementary Dataset 8). Formate is a low-potential reductant that has been argued to support hot spring primary productivity, including in YNP[78,79], which is consistent with the above results. DOC values were significantly higher in AS than in MS and CS (Fig. 2k), consistent with other studies[80], indicating that organic carbon (e.g. formate) would be more readily available in AS and potentially explaining the enrichment of formate oxidation capacity in those springs. Lastly, the capacities for methanol oxidation and methylamine metabolism were both minimally represented among a few mOTUs (Fig. 5; Supplementary Dataset 8) and are consequently not highly relevant mechanisms of energy conservation in high-temperature YNP springs.

Gas-based metabolisms

Recent studies have suggested that microbial metabolisms fueled by gaseous substrates are prevalent in springs that exhibit mixing of water types and that are moderately acidic[8,21,42]. Consistent with the enrichment of WL-encoding MAGs in MS (Supplementary Fig. 17), archaeal MAGs encoding methanogenesis or methane/alkane oxidation pathways have recently been identified and characterized in MS within YNP[8,81]. In the present study, methanogenesis (or methane/alkane oxidation) capacity was only inferred for a single mOTU of the Archaeoglobales (mOTU154), a single mOTU of the Hadarchaeota (mOTU087), and three mOTUs within the Methanomethylicia (mOTU062, 127, and 181), all of which were predominantly present in MS, albeit in low abundances (generally <1.0% relative abundance), with complete absence in AS and near absence in CS also (Fig. 5; Supplementary Dataset 8). Contrasting with previous reports, the capacity for methanogenesis (or methane/alkane oxidation) was not observed in six MAGs from six different hot springs that were highly related (>96–99% AAI) to three previously recovered Korarchaeia MAGs (Ca. Methanodesulfokores washburnensis/NM4/LM09) that were produced from the same Washburn hot spring YNP metagenome[81–83], with the former six MAGs all estimated as 78-94% complete (Supplementary Dataset 2). The Ca. Methanodesulfokores washburnensis organisms were previously suggested to encode the co-occurring capacity to reduce SO_3^{2-} that is coupled to methan/alkan-otrophy. While the SO_3^{2-} reduction capacity was confirmed for the six Ca. Methanodesulfokores washburnensis MAGs of this study (Supplementary Datasets 8-9), none of the MAGs encoded the proteins required for methanogenesis (or methan/alkan-otrophy; e.g. Mcr and

Mtr). The inability to detect genes encoding homologs of proteins involved in methanogenesis affiliated with Ca. Methanodesulfokores washburnensis in any of the MAGs estimated to be nearly complete (or from searches of the unbinned metagenomic data for each of the six springs) suggests an incomplete understanding of the methanogenesis or methan-/alkan-otrophy potential and ecological role of Ca. Methanodesulfokores washburnensis-related organisms within hot springs. Nevertheless, the lack of detection of methane-metabolizing Ca. Methanodesulfokores washburnensis in the MAG or unbinned data for the hot springs analyzed here suggest that they are either very low abundance taxa in YNP hot springs and/or comprise highly genomically variable sub-populations across hot springs.

The co-occurring capacity for both SO_4^{2-} reduction and methanogenesis (or methan/alkan-otrophy) has also been reported for several Archaeoglobales MAGs recovered from the same Washburn hot spring metagenome described above (previously published MAGs LM01 and LM03[82]), in addition to another population exclusively putatively involved in methanogenesis (LM02)[82]. In contrast, two distinct Archaeoglobales OTUs were identified in the present dataset across the 67 metagenomes (mOTU027, $n = 13$ MAGs from 13 springs and mOTU154, $n = 3$ MAGs from three springs), with mOTU027 only encoding the capacity for methanogenesis (or methan-/alkan-otrophy) and mOTU154 only encoding the capacity for SO_4^{2-} reduction (Supplementary Dataset 8). The similarity of the previously described MAGs (LM01 and LM03) was high relative to the 13 exclusively SO_4^{2-} reducing Archaeoglobales MAGs of this study (93–96% AAI), consistent with them being a YNP hot spring-specific metapopulation (Supplementary Dataset 9). However, the McrA from LM01/03 was nearly identical to the McrA of the three exclusively CH_4-metabolizing MAGs identified in this study (99–100% AAI; Supplementary Dataset 9). The three CH_4-metabolizing Archaeoglobales MAGs of this study co-occurred with the SO_4^{2-} reducing Archaeoglobales in all three springs where the former was identified (Supplementary Dataset 8), which may suggest that they are involved in synergistic metabolic interactions. However, the results concurrently suggest that the previously inferred co-occurring capacity for these functions in the same cells to have potentially been artifactual. Nevertheless, these data point to a consistent presence and co-occurrence of CH_4-metabolizing organisms in MS (Fig. 5, Supplementary Fig. 17). CH_4 values were highest in AS and MS, with some of the highest values reported in MS where the CH_4-metabolizing organisms were found (Supplementary Dataset 1), although differences relative to CS were not statistically significant (Fig. 2f). The presence of CH_4 in MS may suggest the widespread potential for anaerobic methan-/alkan-otrophy in these spring types. Such potential is consistent with recent enrichment cultures of methylotrophic methanogenic cultures of Archaeoglobales from YNP[84] in addition to inferences of methylotrophic methanogenesis or alkanotrophic metabolism in taxa related to the Mcr-encoding organisms identified here[85]. The potential for methanotrophy via soluble methane monooxygenases (Mmo) was also statistically enriched in MS and CS (Supplementary Fig. 17) and was moderately abundant in these spring types. Methanotrophy through Mmo is generally considered an aerobic process[86], although the taxa encoding this capacity were largely inferred to be anaerobic, including members of the Desulfurococcales, Nezhaarchaeales, and Thermodesulfobacteria (Supplementary Dataset 8). To our knowledge, nothing is known of this potential in these taxa and warrants further analyses. Nevertheless, given the high levels of CH_4 in MS described above, such metabolisms may be expected for these systems.

H_2 metabolism via [NiFe]- and [FeFe]-hydrogenases was widespread among hot spring populations, although primarily via [NiFe]-hydrogenases (Supplementary Fig. 17). [FeFe]-hydrogenases were statistically enriched in MS and CS, albeit at very low abundances (Supplementary Fig. 17), while [NiFe]-hydrogenases were highly abundant in all spring types, but especially prominent in MS, and to a lesser

extent CS and AS (Fig. 5; Supplementary Fig. 17). [FeFe]-hydrogenases were only present in 31/372 mOTUs and largely within anaerobic bacterial taxa like the Thermotogota, Caldisericota, and Firmicutes, while [NiFe]-hydrogenases were present in 190/372 mOTUs comprising diverse archaeal and bacterial clades (Supplementary Dataset 8). This is consistent with recent analyses showing enrichment of hydrogenases in MS[21] and with geochemical data suggesting H_2 concentrations as highest in MS springs, albeit not statistically significantly higher than in AS or CS (Fig. 2e)[87]. The capacity for aerobic carbon monoxide oxidation (e.g. via aerobic carbon monoxide dehydrogenase, Cox) was statistically enriched in AS and CS communities and mOTUs generally (encoded by 104/372 mOTUs). Cox subunits were also encoded by diverse archaeal taxa in this study, including by Thermoproteales, Nitrososphaeria, Sulfolobales, Desulfurococcales, Gearchaeales, and others (Supplementary Dataset 8), suggesting a widespread ability to capitalize on CO as a reductant and/or carbon source. Despite the enrichment of this function in AS and CS communities, it was nevertheless prevalent across all springs, potentially coinciding with high energetic favorability of CO oxidation across the scale of pH found in hot springs[12].

Sulfur metabolisms

The capacities for SO_3^{2-} or SO_4^{2-} reduction (SR) were widespread among the three spring types (primarily through the presence of dissimilatory sulfite reductases, dsr) (Fig. 5, Supplementary Fig. 17). The taxa encoding DsrAB isoforms were distinct among spring types and the DsrAB isoforms themselves exhibited a pH-dependent distribution, with Thermoproteales (Vulcanisaeta and Caldivirga) and Nitrososphaeria SR inhabiting AS; Thermoplasmatota, unclassified Thermoproteales, Korarchaeales, Archaeoglobales, Gearchaeales, and bacterial SR inhabiting MS; and Caldarchaeales, in addition to diverse bacterial SR taxa inhabiting CS (Supplementary Fig. 17). Dsr has been suggested to have possibly arisen in a moderately thermoacidophilic archaeon[40] and its widespread prevalence in hot spring thermophiles in YNP suggests that SO_3^{2-} or SO_4^{2-} reducing metabolisms are favorable in diverse geochemical environments, despite considerable variation in the availability of SO_3^{2-} and SO_4^{2-} (e.g. Fig. 1c)[40,88]. Nevertheless, the general availability of SO_4^{2-} across all hot spring types due to the input of volcanic sulfur dioxide (SO_2) in deep hydrothermal aquifers likely supports the phylogenetically diverse SR populations within them. In addition to the confirmation of SO_3^{2-} reduction capacity in recently characterized Archaea including the Thermoplasmatota[40], Korarchaeia[83], and Nitrososphaeria[70], the capacity for SO_3^{2-} reduction was also present in several Caldarchaeales and Gearchaeales MAGs that have not been previously characterized (Supplementary Dataset 8; Supplementary Fig. 18). The basal branching of the novel Caldarchaeales and Gearchaeales DsrAB among reductive 'archaeal/bacterial-types' in a phylogenetic reconstruction (Supplementary Fig. 18), along with the inferred inability to reduce SO_4^{2-} by either of these taxa (Supplementary Dataset 8), provide additional support for recently developed hypotheses that SO_4^{2-} reduction among Archaea and Bacteria originated in a thermophilic SO_3^{2-}-reducing archaeal lineage[40,89].

Like SR, the capacity for S^0 oxidation was prevalent in taxa across all spring types (i.e. in 108/372 mOTUs), suggesting that it is a generally important metabolic function of hot spring populations. Although the total sulfur content of AS is higher than in MS and CS, the capacity to oxidize S^0 primarily via genes also involved in thiosulfate ($S_2O_3^{2-}$) oxidation (i.e. sulfur oxidase, sox, genes) was widespread, but statistically enriched in AS (Fig. 5, Supplementary Fig. 17). The taxa encoding S^0 oxidation capacity included Aquificota taxa that are distributed across all spring types, Sulfolobales primarily within AS springs, and several uncultured archaeal taxa found in MS and CS including Bathyarchaeia, Nitrososphaeria (including Caldarchaeales), and Gearchaeales, in addition to uncultured bacterial taxa within the Hydrothermaceae and Calescibacteria groups. The anaerobic metabolism of $S_2O_3^-$ disproportionation was also statistically enriched in MS and CS, largely due to its encoding by Thermodesulfobacteria that characteristically inhabited these spring types, consequently representing a relatively limited metabolism of hot spring populations (Supplementary Dataset 8).

AS were dominated by Sulfolobales (Fig. 4), in addition to subdominant populations of Desulfurococcales, Nitrososphaeria, and Thermoproteales, among others (Fig. 4). Thus, many of the enriched functions within these springs reflected metabolic functions encoded by the above taxa. Sulfide and $S_2O_3^{2-}$ oxidation (that comprised overlapping genes for S^0 oxidation) were particularly prevalent metabolisms among MAGs recovered from AS, along with the capacity for S^0 reduction, consistent with the high total sulfur contents of these spring types (Fig. 5; Supplementary Fig. 17). Sulfide oxidation is a key initial step in the acidification of hot springs (described in detail above) and recent evidence suggests that Sulfolobales can significantly accelerate its oxidation relative to abiotic reactivity[29]. Thus, the widespread capacity for sulfide and sulfur oxidation in AS observed here is consistent with a key role for Archaea in driving the acidification of hot springs[28].

Nitrogen metabolisms

Several nitrogen-related metabolic functions were notably absent among the MAGs analyzed here. The genes encoding the capacity for ammonia (NH_3/NH_4^+) oxidation (ammonia monooxygenase; amo), NO_2^- oxidation, or dinitrogen (N_2) fixation (nitrogenase; nif/anf/vnf) were particularly rare, and the capacity for anammox was not observed at all (Fig. 5). Only 1 mOTU comprising 2 MAGs encoded amo genes and was closely related to the previously characterized NH_3/NH_4^+ oxidizer Candidatus Nitrosocaldus yellowstonii[90]. Given the limited distribution of Ca. Nitrosocaldus to a few CS springs, NH_3/NH_4^+ may not be a widely used reductant in high-temperature YNP springs, despite high NH_3/NH_4^+ availability in many AS springs[91,92]. In contrast to AS, NH_3/NH_4^+ availability is low in most MS/CS springs[91,92], yet the capacity for N_2 fixation to generate bioavailable nitrogen was only identified in three Hydrogenobaculum MAGs (of the 10 Hydrogenobaculum MAGs within mOTU036 only found in AS), in addition to one Ignisphaera MAG (Desulfurococcales order) of mOTU022 (comprising 14 MAGs distributed in MS and CS). The capacity for N_2 fixation has not been previously described in either of these taxa, and this represents the first evidence of putative N_2 fixation in Archaea outside of methanogens/methanotrophs. Notably, the 3 Hydrogenobaculum MAGs that encoded the nif operon were all from 'Figure 8' spring from 3 separate sampling years (2013, 2018, and 2019). Numerous Hydrogenobaculum genomes from YNP hot springs have been previously analyzed that lack nif homologs[33,93], including in 7 other springs of this study where Hydrogenobaculum was present. Thus, the consistent presence of potentially N_2-fixing Hydrogenobaculum in the same spring across multiple years suggests that this capacity may be an adaptation to the specific geochemical or ecological characteristics of that spring. Nevertheless, the limited distribution of nitrogenase among high-temperature YNP springs, in particular in NH_3/NH_4^+-limited CS, suggests that bioavailable nitrogen is generally not limiting to high-temperature spring communities.

The ability to utilize oxidized nitrogen species (e.g. NO_3^-, NO_2^-; nitric oxide, NO; and nitrous oxide, N_2O) was generally more prevalent in MS and CS communities, with dissimilatory nitrate reduction to ammonium, NO_2^- reduction, and N_2O reduction being statistically enriched in those spring types, while NO_3^- and NO reduction was prevalent in all spring types (Supplementary Fig. 19). However, oxidized nitrogen compounds were in very low abundance in all spring types, often being below detection limits (Supplementary Fig. 1). Nevertheless, the reduction of these compounds represents highly energetically favorable metabolisms in most hot springs[12,94], perhaps

explaining the widespread nature of these pathways in MAGs across hot spring types. Consequently, while oxidized nitrogen species may only represent transient sources of energy substrates (or nitrogen sources) for hot spring taxa, they may be particularly useful substrates to capitalize upon when available.

Arsenic and iron metabolisms

Of the few metabolic functions particularly enriched in CS populations, those involved in arsenic transformations were significantly enriched relative to both MS and AS, with enrichment in MS also being significant relative to AS. Aerobic arsenite oxidation (e.g. via Aio enzymatic complexes) and arsenate reduction (e.g. via putative arsenate reducing molybdopterin enzymes) were highly enriched in CS communities (Fig. 5, Supplementary Fig. 19, Supplementary Dataset 8). In addition, the capacity for anaerobic arsenite oxidation via anaerobic arsenite oxidases (Arx) was statistically enriched in CS communities, although the relative abundances of taxa encoding these functions were generally low (Fig. 5, Supplementary Fig. 19, Supplementary Dataset 8). Consistently, the availability of arsenic was significantly higher in MS and CS (Fig. 2j). Genes enabling aerobic arsenite oxidation were prevalent among Aquificota and *Thermus* Bacteria, among others, that were predominant in CS, in addition to several archaeal taxa, including *Pyrobaculum*, Bathyarchaeia, and uncultured Desulfurococcales (Supplementary Dataset 8). In contrast, the potential for anaerobic arsenite oxidation was limited to a few mOTUs primarily within the Caldarchaeles archaeal order and the Armatimonadota bacterial phylum that were abundant in CS. Consistently, Arx homologs related to members of these orders were identified in a previous meta-analysis of YNP hot spring metagenomes[52], suggesting a role for these taxa in arsenic cycling within high-temperature circumneutral hydrothermal waters. The potential for arsenate reduction was also prevalent among numerous Archaea including *Pyrobaculum*, Desulfurococcales, Nitrosophaeria (including the Caldarchaeales), Gearchaeales, and diverse Bacteria including Chloroflexota, Desulfobacterota, Deinococcota, and Bipolaricaulota, among others (Supplementary Dataset 8). Notably, few homologs of canonical arsenate reductase (ArrA) were identified, with nearly all arsenate reduction potential deriving from phylogenetically cohesive, but divergent molybdopterin catalytic subunits implicated in the specific reduction of arsenate in arsenate-reducing *Pyrobaculum* Archaea and arsenate-reducing *Anaeromyxobacter* Bacteria[95,96]. Arsenic in YNP hydrothermal waters derives from high-temperature water-rock interactions with rhyolite in the deep subsurface[52]. Consequently, the prevalence of arsenic metabolism-related adaptations of CS community taxa (and to a lesser extent MS taxa) is consistent with, and reflects, the sourcing of CS waters that are more reflective of deeply sourced hydrothermal aquifers, as described above.

The capacity to oxidize Fe(II) was prevalent in AS populations via several putative iron oxidation homologs[97], albeit the capacity was not statistically significantly enriched; Fig. 5, Supplementary Fig. 19). Nevertheless, iron oxidation potential coincided with the significantly greater availability of Fe(II) in AS springs (Fig. 2i; Supplementary Fig. 3)[22,49,98] due to the leaching of iron from minerals by acid during reactive transport. Although the capacity for Fe(II) oxidation was most prevalent among the Sulfolobales, consistent with metabolisms identified in several Sulfolobales members[74], Fe(II) oxidation potential was also encoded by members of the Nitrososphaeria and Desulfurococcales inhabiting AS springs (Supplementary Dataset 8), suggesting roles for these organisms in iron cycling. Iron reduction was only implicated in a few low-abundance bacterial taxa, suggesting it may not be a particularly prominent metabolism in high-temperature hot springs, despite the widespread availability of oxidized iron minerals at acidic pH. It should be noted that known genetic mechanisms of iron oxidation and reduction are not fully understood. As such, iron-based dissimilatory metabolisms are likely present in more diverse Archaea and Bacteria than currently known, as evinced by recent reports of cryptic iron metabolisms in subsurface-typical taxa[99,100]. Thus, estimates of the prevalence of these activities in the datasets presented here should be considered conservative.

O$_2$ respiration and other metabolisms

The ability to respire O$_2$ was prevalent in taxa in all three spring types, pointing to its potential importance as an oxidant in hot spring communities (Fig. 5; Supplementary Figs. 20; Supplementary Dataset 8), despite that DO was minimally detected or below detection in most springs (Fig. 2b). Given the high energetic favorability of using O$_2$ as an oxidant during respiration[12], the prevalent capacity to use these substrates combined with their low concentrations suggests that cells may preferentially utilize these oxidants when they are available, even if only transiently. In conjunction with the inferred high level of respiratory capacity across spring types, NADH dehydrogenases were encoded by many taxa, but especially in MS and CS, while V-Type and F-Type ATPases followed distributions of the types of taxa that dominated spring types (Fig. 5; Supplementary Fig. 20) (e.g. Archaea in AS and Archaea/Bacteria in MS and CS). In addition, the capacities for chlorite and perchlorate reduction (via chlorite dismutases, Cld, or perchlorate reductase, Pcr, respectively) were particularly prominent across abundant taxa in all three spring types (Fig. 5, Supplementary Fig. 20). Little is known of the prevalence of these metabolisms in high-temperature environments or thermophiles[101]. Nevertheless, the anaerobic respiration of chlorine oxyanions has recently been shown to be broadly distributed across Archaea and Bacteria via genomic analyses[102], suggesting these metabolic capacities are more ubiquitous than previously recognized. During perchlorate reduction to chlorite via Pcr and chlorite dismutation to Cl$^-$, O$_2$ is produced as a byproduct[103]. This process has been recently invoked to support substantial O$_2$ production in subsurface environments that would otherwise be expected to be anoxic[104]. The inverse relationship between temperature and O$_2$ solubility, combined with the low potential for O$_2$ ingassing into spring waters from the atmosphere, would lead to substantial ecological advantages for taxa that encode metabolic processes to generate O$_2$. These observations may explain the widespread prevalence of these enzymes among hot spring taxa in this study, although little is known about chlorine oxyanion concentrations in hot spring waters, nor of in situ microbial chlorine oxyanion reduction at high temperatures, warranting additional research.

Association of geochemistry and evolutionary histories

Given the distinctiveness of microbial communities among geochemical realms and the implied eco-evolutionary dynamics described above, the phylogenetic patterning of the mOTUs was evaluated. A maximum likelihood phylogenomic reconstruction was generated including representative MAGs in addition to 622 other genomes from a previously published bacterial + archaeal phylogenomic reconstruction comprising selections from major bacterial and archaeal order-level lineages[105]. The tree was rooted between the bacterial and archaeal domains and the distance of each MAG to the phylogenetic root was calculated as a proxy for the relative ages of the taxa (i.e. tips; Supplementary Fig. 21), using the root-to-tip distance measure. The distances of tips to the archaeal-bacterial divergence were used to estimate degree of relative divergence from the root. The tree agreed with a previously published phylogeny constructed to identify the phylogenetic placement of major bacterial and archaeal lineages, as evinced by a highly significant level of concordance for the phylogenetic distances of reference taxa in both trees ($n = 622$) (linear regression adj. $R^2 = 0.95$, $p < 0.001$, two-tailed, slope $= 1.30$; Supplementary Fig. 22). Likewise, the topology of the bacterial component of the tree was consistent with previously observed phylogenetic placement of major bacteria bacterial lineages including for deeply-branching Thermotogota
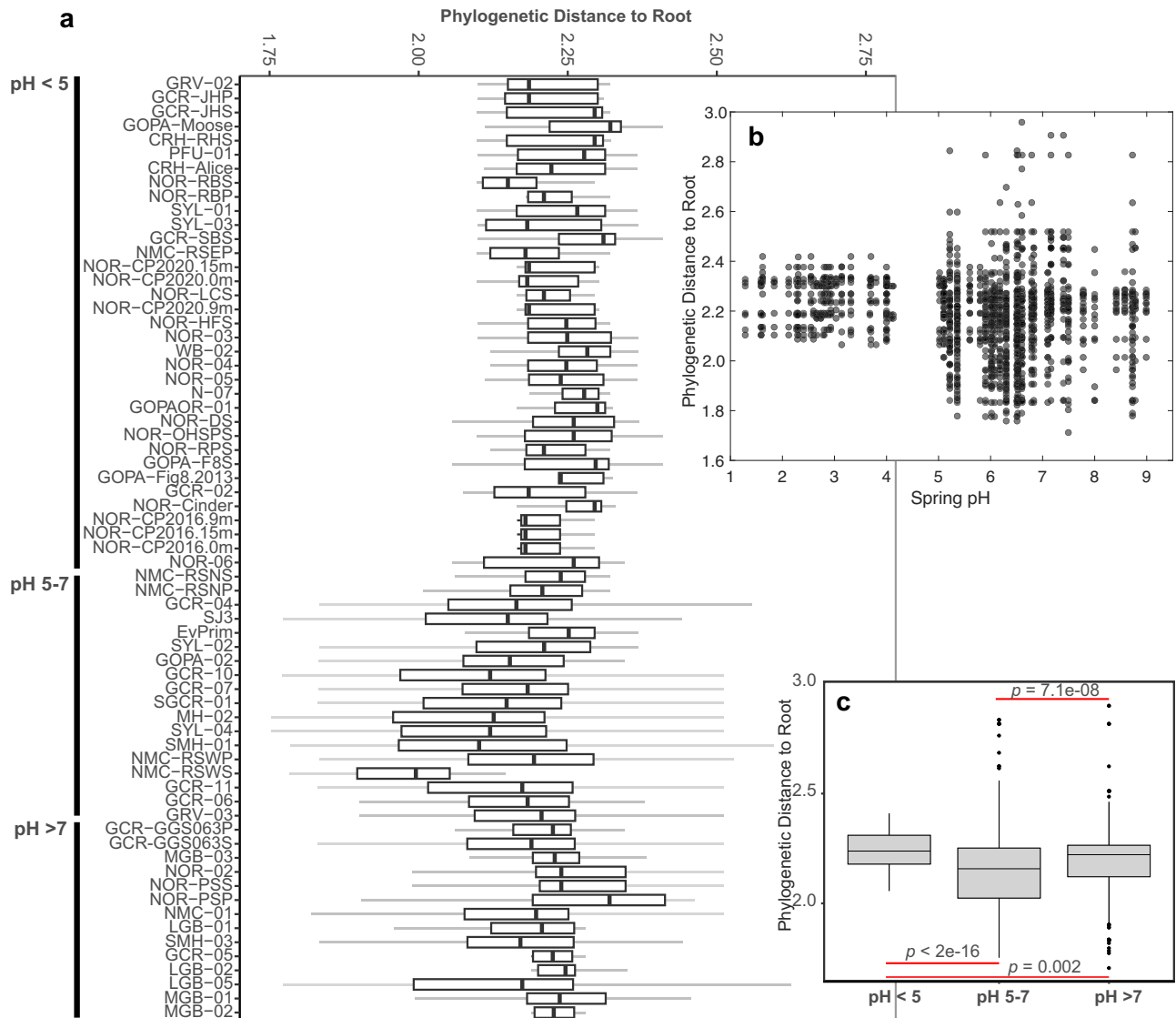
Fig. 6 | Concordance of phylogenomic analyses and ecological distributions of hot spring populations. a Phylogenetic distances of metagenome-assembled-genomes (MAGs) to the phylogenetic root. Distances to the phylogenetic root (i.e. the archaeal-bacterial bifurcation) were calculated for each MAG as the distance of the placement of that MAG to the root in a maximum likelihood (ML) phylogenomic tree (see materials and methods for details). The ML tree contained representatives of OTUs for all bacterial and archaeal MAGs analyzed in this study ($n = 372$) along with 622 other isolate genomes and MAGs from major archaeal and bacterial orders used in a previous phylogenetic analysis of major archaeal and bacterial lineages[105]. The distances calculated for each mOTU (defined at >95% genome homology) were used for all MAGs within that mOTU. Root-to-tip distance distributions are shown for the collection of MAGs from each hot spring community, arranged in order of ascending pH of the spring extending from the top to the bottom of the plot. The hot spring community identifier is shown on the Y-axis. Additional details for each hot spring are provided in Supplementary Dataset 1. Black lines within boxplots

show median values for that hot spring community distribution, the edges of the boxes show the 25th and 75th quartile ranges, whiskers show the range of data. Outliers are not shown to facilitate visualization. **b** Root-to-tip distances for all 1466 MAGs of this study, arranged by the pH of the spring they derive from on the X-axis. **c**) Statistical analysis of the distributions of root-to-tip distances for MAGs within acidic (AS; pH < 5, $n = 298$), mixed (MS; pH 5–7, $n = 840$), and circumneutral/alkaline (CS; pH > 7, $n = 314$) spring types. Boxplots are shown and defined the same as in (**a**), except that outliers are shown as black circles. Differences in overall distributions were statistically assessed by pairwise Wilcoxon rank sum tests with Benjamini & Hochberg multiple comparison correction. The resulting pairwise p-values (two-sided) are shown for each comparison. The distance values for each MAG in association with metagenome origin and taxonomic classification are provided in Supplementary Dataset 2. The phylogenies used to evaluate distances are shown in Supplementary Figs. 21–24 and Supplementary Dataset 11.

and Bipolaricaulota (Acetothermia), followed by Terrabacteria phyla and then Gracilicutes (Supplementary Fig. 23)[105,106]. The general topology of the archaeal phylogeny also reflected previously observed branching orders for major archaeal groups, including a deep-branching placement of the DPANN, followed by Halobacterota (Euryarchaeota) and the TACK + Asgardarchaeota group (Supplementary Fig. 24). The root-to-tip distances generally followed the branching patterns in the phylogenetic trees, with the exception of well-known highly derived clades that exhibited higher

distances (e.g. Patescibacteria and Nanoarchaeota; Supplementary Figs. 25–26).

The distributions of phylogenetic distances significantly varied with pH (Fig. 6; Supplementary Fig. 27). The statistical significance was maintained whether considering Archaea or Bacteria alone, although the trend for Archaea was more significant (Supplementary Fig. 27) and comparisons of MS and CS to AS could not be adequately made for Bacteria given the few bacterial MAGs identified in AS. Likewise, the overall ranges of archaeal and bacterial phylogenetic distances were

similar, with the exception of those of Patescibacteria that were among the highest in the datasets (Supplementary Figs. 25, 27; Supplementary Dataset 2), consistent with recent evidence that they comprise a derived bacterial clade[105]. Thus, the dominance of communities by one or the other domain did not significantly impact observed phylogenetic distance distributions.

AS communities comprised lineages with the largest phylogenetic distances, indicating the presence of relatively later-branching taxa (Fig. 6). These observations are consistent with other phylogenetic estimates for the relatively recent divergence of thermoacidophiles like the Sulfolobales[28,107] that dominate acidic hot spring environments in YNP and in other geothermal systems[58,108]. Likewise, the other Archaea inhabiting AS including members of the Desulfurococcales (*Acidilobus* and *Caldisphaera*; Supplementary Figs. 28–30), Thermoproteales (*Caldivirga*, *Vulcanisaeta*, *Thermoproteus*, and *Thermocladium*) (Supplementary Figs. 28–29, 31), the UBA164 group of Nitrososphaeria (formerly Thaumarchaeota) (Supplementary Figs. 28–29, 32), and the Thermoplasmatales group of Thermoplasmata (Supplementary Fig. 28), in addition to the single acidophilic bacterium, *Hydrogenobaculum* (Supplementary Fig. 33), were all among the later diverging taxa within their higher order taxonomic groups (e.g. orders or classes). These data point to independent diversification of several taxa into acidic niches and that these divergences occurred relatively recently within each lineage. The widespread oxygenation of Earth's atmosphere occurred only at ~2.4 Gya and further oxygenation to near present-day values only occurred ~0.8–0.6 Gya, as reviewed in ref. 31. These changes in Earth history are considered to have significantly altered biogeochemical cycling across Earth and especially, enabling oxidative sulfur cycling[109]. Notably, the organisms that dominate AS (i.e. primarily Sulfolobales) are obligate or facultative aerobes (Supplementary Dataset 8), whose carbon fixation typically relies on the aerobic oxidation of sulfur compounds (e.g. sulfide and S^0) (Fig. 5, Supplementary Fig. 17)[74]. Likewise, acidic hot springs are generated by the oxidation of these same compounds, potentially due to the activity of Sulfolobales or others, as inferred from geomicrobiological studies spanning ~60 years[23–29,41]. It is possible, if not likely, that these lineages and their environments only appeared relatively recently in Earth history as a consequence of Earth's oxygenation. These interpretations are consistent with recent inference that O_2-dependent ammonia oxidizing Archaea evolved upon initial oxygenation of Earth's atmosphere and then diversified into subsequently greater oxygenated fresh- and marine waters only in the last ~1 Ga when O_2 became more widely available[110].

CS also harbored relatively later diverging lineages (Fig. 6). These springs were primarily dominated by *Thermocrinis* Bacteria, *Pyrobaculum* Archaea, and Archaea from the Desulfurococcales and Caldarchaeales orders (Fig. 5; Supplementary Dataset 2) that were also among the later-diverging taxa of their higher order taxonomic groupings (Supplementary Figs. 28–32). In continental geothermal systems, higher pH springs are generally derived from the liquid phase following decompressional boiling and are depleted of volatile gases and oxidants, but replete with solutes due to high-temperature water-rock interactions (Fig. 2), as described above and elsewhere[17,18,24,25]. A typical hallmark of these springs in YNP is the precipitation of silica sinters (e.g. as terraces or mounds) upon their emergence due to cooling of hydrothermal waters supersaturated with respect to silica (Fig. 2l)[24,25]. Many of these springs exhibit minimal mixing with other waters due to silica armoring of the flow paths that fluids take to reach the surface[22,111]. Further, high pH waters originating from the subsurface generally exhibit low DOC concentrations[80] (Fig. 2k) and are generally gas-poor (Fig. 2e–g)[21,87]. Thus, the lack of available oxidants, organic carbon, and gaseous substrates renders these waters energetically limited environments for microbial activity. Indeed, recent studies have suggested that these high-temperature springs only become habitable upon their emergence at the surface that allows for

infusion of atmospheric O_2[22,35]. Specifically, near-surface CS-type waters are dominated by autotrophic obligate aerobes (e.g. *Thermocrinis*) that likely facilitate the presence of heterotrophs (including those inhabiting waters, sediments, and biofilms)[32,33,43]. Given the above observations, the habitability of these springs in the absence of atmospheric O_2 infusion remains unclear. Moreover, of the few types of metabolisms enriched in CS communities in this study was aerobic oxidation of arsenite in addition to arsenate reduction. Arsenite oxidation to arsenate in hot springs is predominantly driven by biological activity[52] like that of *Thermocrinis* that dominated these spring types. Thus, both arsenite oxidation and the generation of arsenate for biological reduction are intrinsically tied to O_2 availability at the surfaces of these springs. Consequently, the relatively later-diverging nature of bacterial and archaeal lineages that inhabit CS may suggest relatively recent adaptation to these environments, perhaps also when atmospheric O_2 became more widely available on Earth. An alternative explanation is that these taxa could have competitively replaced anaerobic taxa that inhabited these environment types once O_2 became available.

In contrast to the AS and CS communities, taxa inhabiting MS generally comprised earlier-diverging lineages (Fig. 6). This observation was apparent when evaluating higher-order taxonomic groupings (e.g. across the class/phylum levels of Archaea; Supplementary Fig. 28), in addition to within lineages (e.g. within the Thermoproteota, Caldarchaeales, and Aquificota; Supplementary Figs. 29–31). This pattern is driven, in part, by the abundance of archaeal lineages in these springs that exhibit smaller phylogenetic distances from the archaeal-bacterial root and have elsewhere been considered early-branching, including the Methanomethylicia (formerly Verstratearchaeota), Bathyarchaeia, and Hadarchaeota (Fig. 5; Supplementary Fig. 28)[112]. The WL pathway was specifically enriched in these spring types, and which is primarily associated with anaerobic Archaea and Bacteria[77]. The WL pathway has been suggested to be the oldest carbon fixation pathway in Archaea and Bacteria due to its presence in deeply branching lineages of both domains[113–115], which is consistent with the smallest phylogenetic distances to the root being in MS and the enrichment of this pathway in MS communities. Notably, springs that are only moderately acidic are rare relative to the more prominent AS and CS types in continental hydrothermal systems[18,30,37]. Many of the MS of this study contained visibly black sediments (Supplementary Dataset 10) typical of sulfide-rich hot springs and the presence of iron-sulfide minerals found in anoxic high-temperature environments[116]. Further, many of these springs exhibited among the lowest measured DO concentrations (Fig. 2b). Intriguingly, the sediment community of one of the MS that was sampled in a previous study, 'Roadside West' spring[42], exhibited among the lowest overall distribution of phylogenetic distances, while the taxa in the water community from the same spring (NMC-RSWS and NMC-RSWP, respectively, Fig. 6a) exhibited much larger distances. Given that the primary difference in the geochemistry of water overlying sediments is likely the redox state and the presence of redox-active minerals in sediments, these results support that the oxidation state of hot spring environments plays a significant role in establishing the phylogenetic patterns described above.

The separation of fluids into a vapor and liquid phase during decompressional boiling is a physical process that is expected to universally occur in continental hydrothermal systems both today and in the geologic past. While contemporary hot springs exhibit bimodal pH distributions due to the O_2-dependent oxidation of H_2S, the absence of near-surface oxygenated waters would be expected to lead to an absence of highly acidic low-pH waters (i.e. AS) in continental hydrothermal systems, given current models of hot spring formation[18,24,25]. Consequently, the largely suboxic MS may represent contemporary analogs for understanding microbial systems resultant from incomplete oxidation of vapor phase gases following condensation with meteoric water. This hypothesis is consistent with those invoking

anoxic vapor-dominated continental geothermal systems on early Earth as potential sites for the origin of life[117] as well as fossil evidence from the Dresser Formation, Australia, suggesting the presence of microbial life in vapor-sourced hot springs at -3.5 Ga[118]. Anaerobic metabolisms are enriched among Archaea and Bacteria inferred to be early-diverging[6] and thus, may help explain the phylogenetic patterning and ecological distributions observed herein, where relatively earlier-diverging lineages were present in largely anoxic or suboxic MS relative to AS and CS.

Discussion

Hot springs have long served as analogs to understand the environmental conditions and metabolisms that supported the earliest life on Earth. However, hot springs vary widely in their geochemical and microbiological composition, rendering it unclear the extent to which contemporary hydrothermal environments actually reflect the types of environments that might have supported early life on Earth. Here, a comprehensive and integrated assessment of geochemical, physiological, and phylogenetic data of YNP high-temperature springs and their communities revealed that the two most abundant spring types in contemporary continental hydrothermal environments (acidic and circumneutral/alkaline springs) host relatively later-branching archaeal and bacterial lineages, while also hosting communities that are especially dependent on atmospheric O_2 for their functioning. In contrast, moderately acidic springs (pH 5–7) that are generally rare in continental hydrothermal systems today hosted relatively earlier-branching lineages comprising populations especially supported by anaerobic, gas-dependent metabolisms. Moderately acidic springs are formed by mixing of volatile (e.g. H_2S, H_2, CO_2 CH_4) rich gas with meteoric or hydrothermal waters and represent precursors to the formation of acidic springs (pH < 4). However, the transition from moderately acidic (pH 5–7) conditions to acidic springs (pH < 4) requires sufficient oxidizing power (e.g. O_2 or O_2-derived oxidation products such as Fe(III)) to generate strong acid (e.g. sulfuric acid) and long enough residence times to allow for acidification to occur. In many instances, such moderately acidic springs form at higher elevations in YNP, likely facilitating lower water residence times[20,21] that enables incomplete acidification and suggests a geomorphological component to the geochemical-microbiological associations identified herein. Consequently, prior to the emergence of oxygenic photosynthesis and the generation of widely available O_2 during Earth history, moderately acidic springs were likely much more prevalent. Thus, the generally anoxic, gas-rich conditions observed in contemporary moderately acidic springs may better reflect conditions of such springs. Infusion of O_2 from the atmosphere or by input of O_2-containing meteoric water is unavoidable in hot spring environments today. Nevertheless, moderately acidic springs in contemporary continental geothermal fields and the microbial populations they host may serve as useful platforms to understand volcanic gas-influenced, similar springs that may have been more prevalent on a mostly anoxic early Earth.

The results of this study provide insight into the distribution of genomic biodiversity, functional potential, and phylogenetic patterning of thermophilic Archaea and Bacteria as a function of geochemical variation in YNP hot springs. It should nevertheless be noted that the YNP geothermal system is a singular example that has arisen primarily due to rhyolitic volcanism. Consequently, similar studies should be conducted in other geologic contexts, although the prevailing geophysical and geochemical processes that lead to geochemical variation in YNP should be similar globally and should lead to similar eco-evolutionary feedbacks within local environments. Consistently, our recent 16S rRNA gene-based analysis of hot spring community composition among globally distributed, geologically distinct settings demonstrated similar co-variation in geochemical-taxonomic composition patterns across systems[61]. These collective results suggest that

complex influences from geologic settings, dispersal limitation, and localized geologic/hydrologic characteristics likely influence observed biogeographic patterns of global hot spring biodiversity. Notably, tectonic setting has recently been shown to significantly influence coordinated geochemical and microbiological variation observed among continental[61,119,120] and deep-sea[62] hydrothermal systems. Additional targeted comparisons of such systems may provide further insights into the coordinated evolution of thermophiles and their hydrothermal environments across Earth history and across global hydrothermal contexts.

Methods

Sampling and geochemical analyses

Hot spring surface sediment samples were sterilely collected for molecular analyses from 34 springs in 2019 and 2020 (Supplementary Datasets 1 and 10). Data from 19 additional springs comprising 35 total samples (20 sediment community and 15 water community samples) (Supplementary Dataset 1) from our other studies were included in the analyses and were similarly sampled and processed. Specific details for each metagenome are provided in the original publishing article that is indicated in Supplementary Dataset 1. For the sediment samples newly described here, they were immediately placed on dry ice for transport to the laboratory, followed by subsequent storage at −80 °C. On-site measurements were made in waters directly above sediment sampling locations for temperature, pH, and conductivity using portable instruments, in addition to measurements of Fe(II), total sulfide (S^{2-}), and total dissolved silica using a field spectrophotometer (Hach DR890) and colorimetric assays as previously described[63,121]. Dissolved oxygen (DO) concentrations were measured on-site using a high-temperature PSt3 oxygen dipping probe and a Fibox 4 DO instrument (PreSens, Regensburg, Germany)[121]. Waters were filtered with 0.22 μm pore size filters (Pall) and preserved for geochemical analyses including anion, trace element, and δD/δ18O water isotopes, as previously described, including immediate refrigeration of samples and acidification of waters for trace element analysis[63,121]. Waters were similarly filtered using 0.22 μm filters and preserved for cation, dissolved inorganic carbon (DIC), dissolved organic carbon (DOC), and carbon isotope analyses. Briefly, major cations (total dissolved lithium, sodium, potassium, calcium, and magnesium) were analyzed at the Montana Bureau of Mines & Geology (MBMG) Analytical Laboratory using a Thermo Scientific iCAP 6000 Series inductively coupled plasma-optical emission spectrometer (ICP-OES, EPA method 30.0). Dissolved inorganic (DIC) and organic carbon (DOC) concentrations were measured using an Aurora 1030 W Total Carbon Analyzer. All samples were analyzed in triplicate and the concentrations determined using a calibration curve generated through the analysis of standard solutions made with lithium carbonate/sodium bicarbonate for DIC and potassium hydrogen phthalate/sucrose for DOC. The δ13C values were acquired using a Picarro δ13C-CO_2 analyzer coupled to the Aurora 1030 W. The error for total DIC, DOC, and δ13C values were reported as the standard deviation of the three replicates of each sample. Dissolved gasses were collected by pumping water from depth in gas-tight tubing, followed by exsolving gasses into a - 10 mL ultrapure N_2 gas bubble in a syringe with 100 mL of spring water. Triplicate N_2/dissolved gas mixtures were then injected via displacement into sealed 20 mL glass vials containing a saturated NaCl solution and stored upside down to avoid leakage through the rubber stopper of the vial. Gas (H_2, CH_4, and CO_2) concentrations were then analyzed on a gas chromatograph (model SRI 8610 C, SRI instruments, Torrance, CA), as previously described[122]. Gas concentrations were calculated based on reference to standard curves and converted to concentrations based on Henry's Law, as previously described[123]. A geologic map was constructed in ARCGis using datasets from the National Park Service (NPS) Geologic Resources Inventory (GRI) program, 20200616, Digital Geologic-GIS Map of the Yellowstone National Park and Vicinity,

Wyoming, Montana and Idaho (NPS, GRD, GRI, YELL, YELL digital map) adapted from U.S. Geological Survey maps by Christiansen, Blank, Prostka, Smedes, Pierce, the U.S. Geological Survey, Elliot, Nelson, Wahl, Witkind, Love and others (1956–2007), and a Montana Bureau of Mines and Geology map by Berg, Lonn and Locke (1999). Auto-correlation among geochemical variables was evaluated using the 'rcorr' function of the Hmisc package (v.4.6-0; https://CRAN.R-project.org/package=Hmisc) for R using Pearson correlation values. Correlation plots were generated using the corrplot function of the corrplot package for R (v.0.92; https://r-project.org/web/packages/corrplot/).

Metagenomic library preparation, sequencing, and processing
DNA extractions were conducted as previously described[35]. Briefly, at least duplicate extractions were conducted from ~0.5 g aliquots of sediments using the FAST DNA Spin Kit for Soil (MP Biomedicals, Irvine, CA) following the manufacturer's protocols. Extracts were then pooled as needed to achieve sufficient DNA for shotgun metagenomics analyses at the Genomics Core Facility at the University of Wisconsin-Madison on a single lane of the Illumina NovaSeq S4 platform (2×150 bp paired-end reads). Metagenomic libraries were sequenced at a depth of ~70–100 × 10^6 quality-filtered reads individually, although three samples contained $< 65 \times 10^6$ quality-filtered reads due to lower library yields (Supplementary Dataset 1).

Reads were quality-filtered and sequence adapters removed using the TrimGalore v.0.6.0 (https://github.com/FelixKrueger/TrimGalore) program and the Cutadapt pipeline v.2.1.0 with default parameters[124]. Quality-filtered reads were first down-sampled using the Bbnorm script (https://github.com/BioInfoTools/BBMap; v.38.87) to improve assemblies[41]. The normalized reads were then assembled with the MetaSPAdes (v.3.14.0) assembler[125] using default parameters. Assembled contigs from the best quality assembly were then used for metagenome-assembled-genome (MAG) binning using the MetaWRAP v.1.3.2 pipeline[126]. The binning pipeline first incorporates read-mapping to assembled contigs with the BWA aligner (v.0.7.17)[127]. Tetranucleotide frequency distributions and coverage profiles were then used to independently bin contigs with the metaBAT v.2[128], MaxBin v.2[129,130], and CONCOCT v.1.1.0[130] algorithms, specifying a length (-l) of 2500. The bin_refinement module of MetaWRAP was then used to identify the highest quality individual MAGs based on completeness and contamination estimates via CheckM v.1.1.3 and considering bins derived from each individual binning algorithm and from combinations of bin outputs. Protein coding genes within the MAGs were identified and annotated using the prokka pipeline (v.1.14.5)[131] with protein prediction conducted with Prodigal (v.2.6.3)[132]. The relative abundances of MAGs were estimated based on read mapping of quality-filtered reads to the MAG assemblies using the CheckM (v.1.1.3) coverage and profile functions. Taxonomic classifications were conducted using the genome taxonomy database (GTDB) classify workflow within the GTDB-tk program (v.1.3.0)[133]. Despite sampling springs with conditions that should preclude photosynthetic organisms, several low-abundant MAGs affiliated with known photosynthetic lineages were recovered. Those MAGs, along with low-abundance common contaminants of sequence library preparations[134], were not included in downstream analyses. A total of 30 MAGs were removed, including seven associated with photosynthetic bacteria (Cyanobacterota or Chloroflexota: relative abundances of 0.09–2.4%), and 23 from common contaminants (*Ralstonia* and Propionibacterales: relative abundances of 0.06–2.7%). The percentage of reads mapped to the MAG assemblies from each metagenome for the newly described metagenomes was 70.1% on average (range of 48–84%), while that of the previously published metagenomes was 58% on average (range of 20-93%) (Supplementary Dataset 1). The taxonomic compositions of MAG assemblies and unprocessed reads from each metagenome were also analyzed and compared using the SingleM platform (v.0.15.0) and the 'pipe' function with default parameters[135]. The genomic coverage

values for each classification were normalized within each metagenome to calculate relative abundance estimates for a given classification label. To evaluate the concordance of taxonomic composition profiles from the MAG-based datasets with profiles from the raw reads alone, the relative abundances of the 1,022 MAGs newly reported in this study were statistically compared against the estimated relative abundances of the same taxonomic classification among the raw read datasets. The R214 GTDB version was used for the classifications of both the reads and MAGs. Where MAGs were assigned multiple taxonomic classifications (e.g. at the species rank or only at the genus rank), the classification that was most represented (based on percentage of contigs) in the MAG assembly was chosen. If an absolute difference in relative abundance between the read-based and MAG-based classification estimates was >10%, the results were manually inspected to verify the discrepancy, and curated if necessary. The estimated relative abundances for each taxonomic classification in the read-based and MAG-based datasets were statistically compared using a linear regression in the R base package software platform.

Diversity analyses
Metagenomic operational taxonomic units (mOTUs) were identified by first calculating the average nucleotide identities (ANIs) among the curated MAGs from all springs ($n = 1466$) using the fastANI program (v.1.32)[136]. MAGs were not generated from the previously published Old Faithful and Spouter Geyser samples for reasons indicated in the original report[43]. The ANI percentages were converted to dissimilarity values by subtracting the pairwise ANI values from 1 (i.e. identical genomes were given scores of 0.0 and genomes that did not share enough ANI to assign a value were given scores of 1.0). The ANI dissimilarity matrix was then clustered at the 0.05 distance level (i.e. 95% similarity in whole-genome ANI) using the 'cluster' command of the mothur program (v.1.42.1)[137]. The 95% ANI level was used because it corresponds to commonly used bacterial and archaeal species-level thresholds[54]. Rarefaction curves considering all mOTUs together were also constructed in mothur. Whole-metagenome sequence diversity was calculated using a bin-independent approach via the Nonpareil (v.3.304)[138] metric and the quality-filtered reads for each metagenome. Briefly, the N_d sequence diversity metric is derived from Nonpareil sequencing coverage curves and estimates the level of sequence redundancy within a metagenomic dataset to approximate genomic diversity within a metagenome[138].

Between-sample mOTU diversity was evaluated based on the relative abundances of mOTUs among sites and the Bray-Curtis dissimilarity metric and non-metric multidimensional scaling (NMDS), as implemented in the vegan package (v.2.5-7)[139] for R (v.4.0.4)[140]. The association of community composition with environmental variables was assessed by fitting the environmental parameter data to the NMDS ordination using the envfit function of vegan with removal of data containing missing values. mOTU co-occurrence networks were constructed using Pearson correlation coefficients between mOTU pairs that were calculated based on their estimated relative abundances across sites. Only mOTUs identified in >1 site were used for the analyses. Pearson correlation coefficients and corresponding statistical significance (p) values were calculated using the rcorr function for R. The correlation matrix was used to identify strong correlations of mOTU abundances ($p < 0.001$ and $|r| > 0.6$). The resulting 1,023 mOTU correlations were used as edges for a co-occurrence network within the Cytoscape (v.3.8.2)[141] software suite. The network was visualized using the edge-weighted algorithm and p values as the weighting metric. The networks were visualized with each node representing an mOTU that is colored by the average pH of the springs where they were identified. Sub-networks that were not connected to others and with <3 nodes were removed to simplify visualization. mOTU sample breadth (as a function of spring pH) was visualized using the

'geom_density_ridges' function of the ggridges package for R (v.0.5.4).

Functional annotations

Proteins encoded by the MAGs were subjected to initial functional annotation and mapping to metabolic pathways within the Kyoto Encyclopedia for Genes and Genomes (KEGG) database[142] using the METABOLIC software program (v.4.0)[143] and a module identification default cutoff value of 0.75. The presence of several functions were then manually curated following initial identification including: 1) the presence of nitrogenase (Nif) modules was confirmed by evaluating MAGs for the presence of *nifHDK* operons on scaffolds; 2) the catalytic directionality of dissimilatory sulfite reductases (Dsr; i.e. either functioning in sulfite (SO_3^{2-}) reduction or S^0 oxidation) was evaluated by phylogenetic analysis as previously described[40]; 3) instances of the capacity for sulfate reduction in the absence of sulfite reduction capacity were removed; 4) the use of bd-type ubiquinol reductases for O_2 respiration in Archaea were not considered, given a lack of clarity in their functionalities for archaeal respiration[144]; 5) [NiFe]- and [FeFe]-hydrogenases were supplemented by BLAST identification of diverse large subunit (LSU) homologs against the datasets and checked for conserved CXXC motifs as previously described[145,146] and with reference to the HydDB platform[147]; and 6) the presence of the Wood-Ljungdahl (WL) carbon fixation pathway was confirmed by the presence of most of the carbon monoxide dehydrogenase/acetyl-CoA synthase (CODH/Acs) subunits, in addition to most of the proteins within the bacterial or archaeal western branches of the pathway. Partial WL pathways were considered present for archaeal groups that have been shown to comprise various components of WL pathway western branches[76].

Several additions were amended to the METABOLIC-based KEGG functional annotations, including the presence of 1) O_2 respiration proteins encoded by Sulfolobales (*Desulfurolobus* oxidases; DoxBCE)[74]; 2) thiosulfate:quinone oxidoreductase proteins encoded by acidophiles and others (DoxAD)[74]; 3) iron reduction or oxidation proteins, as annotated with the FeGenie software program[97]; 4) S^0 oxidation capacity via a heterodisulfide reductase operon ($hdrAB_1C_1B_2C_2$) that exhibits a conserved structure[148]; 5) S^0 reduction capacity via a putative NAD(P)H sulfur oxidoreductase (NSR) complex and associated ferredoxin:NAD(P)$^+$ oxidoreductase (FNOR) complex[149]; and 6) putative arsenate reduction genes encoding molybdopterin oxidoreductases that are phylogenetically related to tetrathionate reductase-like genes, but that have been implicated in archaeal[95] and bacterial[96] arsenate specific reduction. Molybdopterin oxidoreductases comprise a large family of proteins with diverse functionalities and whose functionalities are considered phylogenetically cohesive with catalytic subunit amino acid sequences[150]. Consequently, a phylogenetic analysis was conducted using catalytic subunits from major molybdopterin oxidoreductase groups, in addition to putative arsenate-respiring homologs described above, and tetrathionate reductase homologs used elsewhere[96]. Details of the phylogenetic analyses are provide in the below section. The functional compositions for all MAGs within a metagenome were statistically compared using NMDS ordinations, as described above for the taxonomic compositions of communities. In addition, the environmental data were fit to the NMDS ordination, as also described above, to assess the association of geochemistry and functional compositional variation.

Functional categories in the METABOLIC output were not included in visualization or downstream analyses if evidence for their presence in any of the MAGs was not identified. To achieve conservative estimates of the presence of functions and mitigate potential artefactual attribution of functions to taxa, OTUs with ≥3 MAGs that only harbored 1 MAG encoding a particular function were not considered to encode that function, unless previously published data otherwise suggested the function to actually be encoded by the taxa. The

exception to this caveat was nitrogenase-encoding genes identified in 1 Desulfurococcales MAG that was considered non-artefactual based on comparison to other datasets (described in the results). To assess whether the functional profiles constructed from MAGs deviated significantly from that present in entire metagenomes, metabolic annotations were also evaluated for the entire metagenome assemblies (i.e. not the MAG-based datasets) using the METABOLIC platform, as described above, but considering all 315 functions. The numbers of hits to a given function across the entire metagenome assembly and the sum of the MAGs in that same metagenome were then statistically compared using a linear regression. Only the 34 newly described metagenomes of the present study were compared against the metagenomes to control against variation in metagenomic assemblies based on sequencing depths, sequencing platform, and other factors. The profiles generated from the MAGs and entire metagenomes for the newly described datasets were also statistically compared using NMDS ordinations, as described above, but after first normalizing the numbers of functional hits in each profile to the total in that profile to mitigate artefactual comparisons due to diversity and sequencing depth differences. Statistical comparisons of summed relative abundances for each metagenome among spring types were conducted using pairwise Wilcoxon rank sum tests in the base R stats package (two-sided significance testing), with Benjamini & Hochberg correction for multiple comparisons.

Phylogenetic analysis

A bacterial and archaeal phylogenomic reconstruction was generated using a concatenation of 30 proteins encoded by housekeeping genes including ribosomal proteins ($n = 27$) and RNA polymerase subunits ($n = 3$) that were identified using the markerfinder pipeline[151]. To enable reasonable phylogenetic computational times, representatives from each of the 372 mOTUs were selected for phylogenomic analysis in conjunction with 622 reference genomes from the major orders of Archaea and Bacteria. The 622 reference genomes were the same as used in a previous phylogenomic analysis conducted to establish the phylogenetic placement of major archaeal and bacterial lineages using a balanced taxonomic sampling across orders[105]. Additional reference genomes from the Thermotogota were also included since they have been previously shown as one of the deepest-branching bacterial lineages[105,106]. The markerfinder script (https://github.com/faylward/markerfinder) was used to search genome assemblies for the 30 universal genes. The individual protein datasets were aligned with ClustalO (v.1.2.4)[152] and concatenated. The concatenated alignment was then subjected to trimming using trimal (v.1.4.rev22) by removing alignment sites with gaps in >90% of the sequences (e.g. -gt 0.1)[153]. The concatenated alignments were subjected to Maximum Likelihood phylogenetic reconstruction using IQ-TREE (v.1.6.12)[154] and the LG + F + I + G4 amino acid substitution model based on the model testing function, 'TEST' within IQTREE. One thousand ultrafast bootstraps were used to evaluate branch support and 10 independent phylogenetic runs were used to identify the optimal tree. The consensus tree that exhibited the highest likelihood was rooted at the bifurcation between bacterial and archaeal lineages for subsequent visualization and analyses. The tree is available as Supplementary Dataset 11. To proxy the relative ages of phylogenetic lineages, the phylogenetic distance of each tip to the root was calculated across the entire phylogenetic tree using the distroot function of the adephylo package for R (v.1.1-13). To quantitatively evaluate agreement with robustly supported published archaeal+bacterial phylogenies, the root-to-tip distances were also calculated from the balanced order final tree previously published with the reference genomes used here[105]. The distances were then statistically compared via linear regression against the values obtained for the same genomes in the phylogenetic analysis of this study. The molybdopterin phylogenetic analysis was conducted as described for the phylogenomic analyses, except that the

substitution model chosen for analysis was the LG + F + R7 substitution model and removal of alignments with <50% of the median residue count for the entire dataset.

Reporting summary

Further information on research design is available in the Nature Portfolio Reporting Summary linked to this article.

Data availability

All metagenomic assembly and individual MAG sequence data, in addition to annotation and associated metadata that were generated for this study are publicly available in the Integrated Microbial Genomes (IMG) M/ER database under accessions provided for each metagenome or MAG, as listed in Supplementary Datasets 1 and 2. Sequence read data are available in the NCBI database under the bioproject accession PRJNA791658. The MAG sequence data from the previously published metagenomes are also available under NCBI bioproject accessions or IMG accessions given for each dataset in Supplementary Dataset 1. Source data locations for all figures are indicated in the corresponding figure legends and are either present in Supplementary Datasets or within the accompanying Source Data file. Source data are provided with this paper.

References

1. Knoll, A. H. & Nowak, M. A. The timetable of evolution. *Sci. Adv.* **3**, e1603076 (2017).
2. Anbar, A. D. Oceans. Elements and evolution. *Science* **322**, 1481–1483, (2008).
3. David, L. A. & Alm, E. J. Rapid evolutionary innovation during an Archaean genetic expansion. *Nature* **469**, 93–96, (2011).
4. Djokic, T., Van Kranendonk, M. J., Campbell, K. A., Walter, M. R. & Ward, C. R. Earliest signs of life on land preserved in ca. 3.5 Ga hot spring deposits. *Nat. Commun.* **8**, 15263 (2017).
5. Schopf, J. W. Microfossils of the Early Archean Apex chert: new evidence of the antiquity of life. *Science* **260**, 640–646, (1993).
6. Weiss, M. C. et al. The physiology and habitat of the last universal common ancestor. *Nat. Microbiol.* **1**, 16116 (2016).
7. Leng, H., Wang, Y., Zhao, W., Sievert, S. M. & Xiao, X. Identification of a deep-branching thermophilic clade sheds light on early bacterial evolution. *Nat. Commun.* **14**, 4354 (2023).
8. Colman, D. R., Lindsay, M. R. & Boyd, E. S. Mixing of meteoric and geothermal fluids supports hyperdiverse chemosynthetic hydrothermal communities. *Nat. Commun.* **10**, 681 (2019).
9. Power, J. F. et al. Microbial biogeography of 925 geothermal springs in New Zealand. *Nat. Commun.* **9**, 2876 (2018).
10. Hugenholtz, P., Pitulle, C., Hershberger, K. L. & Pace, N. R. Novel division level bacterial diversity in a Yellowstone hot spring. *J. Bacteriol.* **180**, 366–376 (1998).
11. Barns, S. M., Fundyga, R. E., Jeffries, M. W. & Pace, N. R. Remarkable archaeal diversity detected in a Yellowstone National Park hot spring environment. *Proc. Natl Acad. Sci. USA* **91**, 1609–1613 (1994).
12. Shock, E. L. et al. Quantifying inorganic sources of geochemical energy in hydrothermal ecosystems, Yellowstone National Park, USA. *Geochim Cosmochim. Ac* **74**, 4005–4043 (2010).
13. Boyd, E. S., Fecteau, K. M., Havig, J. R., Shock, E. L. & Peters, J. W. Modeling the habitat range of phototrophs in Yellowstone National Park: toward the development of a comprehensive fitness landscape. *Front. Microbiol.* **3**, 1–11 (2012).
14. Cox, A., Shock, E. L. & Havig, J. R. The transition to microbial photosynthesis in hot spring ecosystems. *Chem. Geol.* **280**, 344–351 (2011).
15. Castenholz, R. W. The effect of sulfide on the blue-green algae of hot springs II. Yellowstone National Park. *Micro Ecol.* **3**, 79–105 (1977).
16. Brock, T. D. Microorganisms adapted to high temperatures. *Nature* **214**, 882–885, (1967).
17. Fournier, R. O. Geochemistry and dynamics of the Yellowstone-National-Park hydrothermal system. *Annu Rev. Earth Planet Sci.* **17**, 13–53 (1989).
18. Arnórsson, S., Stefánsson, A. & Bjarnason, Jn. O. Fluid-fluid interactions in geothermal systems. *Rev. Miner. Geochem.* **65**, 259–312 (2007).
19. Holland, H. D. Some applications of thermochemical data to problems of ore deposits; [Part] 2, mineral assemblages and the composition of ore forming fluids. *Econ. Geol.* **60**, 1101–1166 (1965).
20. Lowenstern, J. B., Bergfeld, D., Evans, W. C. & Hunt, A. G. Origins of geothermal gases at Yellowstone. *J. Volcano Geoth. Res.* **302**, 87–101 (2015).
21. Lindsay, M. R. et al. Probing the geological source and biological fate of hydrogen in Yellowstone hot springs. *Environ. Microbiol.* **21**, 3816–3830 (2019).
22. Sims, K. W. et al. The dynamic influence of subsurface geological processes on the assembly and diversification of thermophilic microbial communities in continental hydrothermal systems. *Geochim. Cosmochim. Acta* **362**, 77–103 (2023).
23. White, D. E., Keith, T. E. C. & Hutchinson, R. A. The geology and remarkable thermal activity of Norris Geyser Basin, Yellowstone National Park, Wyoming. U.S. Gol. Surv. Prof. Pap., 1456 (1988).
24. Nordstrom, K. D., Ball, J. W. & McCleskey, R. B. Ground water to surface water: chemistry of thermal outflows in Yellowstone National Park in *Geothermal biology and geochemistry in Yellowstone National Park* (eds. W. P. Inskeep & T. R. McDermott) 73–94 (Montana State University, 2005).
25. Nordstrom, D. K., McCleskey, R. B. & Ball, J. W. Sulfur geochemistry of hydrothermal waters in Yellowstone National Park: IV Acid-sulfate waters. *Appl. Geochem.* **24**, 191–207 (2009).
26. Mosser, J. L., Mosser, A. G. & Brock, T. D. Bacterial origin of sulfuric acid in geothermal habitats. *Science* **179**, 1323–1324 (1973).
27. Brock, T. D. & Mosser, J. L. Rate of sulfuric-acid production in Yellowstone National Park. *Geol. Soc. Am. Bull.* **86**, 194–198 (1975).
28. Colman, D. R. et al. Geobiological feedbacks and the evolution of thermoacidophiles. *ISME J.* **12**, 225–236 (2018).
29. Fernandes-Martins, M. C., Colman, D. R. & Boyd, E. S. Sulfide oxidation by members of the Sulfolobales. *PNAS Nexus* **3**, pgae201 (2024).
30. Brock, T. D. Bimodal distribution of pH values of thermal springs of the world. *Geol. Soc. Am. Bull.* **82**, 1393 (1971).
31. Lyons, T. W., Reinhard, C. T. & Planavsky, N. J. The rise of oxygen in Earth's early ocean and atmosphere. *Nature* **506**, 307–315, (2014).
32. Meyer-Dombard, D. R. et al. Hydrothermal ecotones and streamer biofilm communities in the Lower Geyser Basin, Yellowstone National Park. *Environ. Microbiol.* **13**, 2216–2231 (2011).
33. Takacs-Vesbach, C. et al. Metagenome sequence analysis of filamentous microbial communities obtained from geochemically distinct geothermal channels reveals specialization of three Aquificales lineages. *Front. Microbiol.* **4**, 84 (2013).
34. Mitchell, K. R. *Controls on microbial community structure in thermal environments; exploring Bacterial diversity and the relative influence of geochemistry and geography* Ph.D. thesis, University of New Mexico, (2009).
35. Fernandes-Martins, M. C. et al. Ecological dichotomies arise in microbial communities due to mixing of deep hydrothermal waters and atmospheric gas in a circumneutral hot spring. *Appl. Environ. Microbiol.* **87**, e0159821 (2021).
36. Stefánsson, A. et al. Quantifying mixing, boiling, degassing, oxidation and reactivity of thermal waters at Vonarskard, Iceland. *J. Volcano Geoth. Res.* **309**, 53–62 (2016).

37. Amenabar, M. J., Urschel, M. R., & Boyd, E. S. Metabolic and taxonomic diversification in continental magmatic hydrothermal systems in *Microbial Evolution Under Extreme Conditions*. 57–95 (De Gruyter, Berlin, 2015).

38. Damer, B. & Deamer, D. The hot spring hypothesis for an origin of life. *Astrobiology* **20**, 429–452 (2020).

39. Allen, E. T. & Day, A. *Hot Springs of the Yellowstone National Park*. (Carnegie Institute of Washington Publications, 1935).

40. Colman, D. R. et al. Phylogenomic analysis of novel Diaforarchaea is consistent with sulfite but not sulfate reduction in volcanic environments on early Earth. *ISME J.* **14**, 1316–1331 (2020).

41. Colman, D. R., Amenabar, M. J., Fernandes-Martins, M. C. & Boyd, E. S. Subsurface Archaea associated with rapid geobiological change in a model Yellowstone hot spring. *Commun. Earth Environ.* **3**, 205 (2022).

42. Fernandes-Martins, M. C., Colman, D. R. & Boyd, E. S. Relationships between fluid mixing, biodiversity, and chemosynthetic primary productivity in Yellowstone hot springs. *Environ. Microbiol.* **25**, 1022–1040 (2023).

43. Keller, L. M., Colman, D. R. & Boyd, E. S. An active microbiome in Old Faithful geyser. *PNAS Nexus* **2**, pgad066 (2023).

44. Christiansen, R. L. The Quaternary and Pliocene Yellowstone Plateau volcanic field of Wyoming, Idaho, and Montana. U.S. Geol. Surv. Professional paper, 729–72, (2001).

45. Larson, P. B. et al. A preliminary study of older hot spring alteration in Sevenmile Hole, Grand Canyon of the Yellowstone River, Yellowstone Caldera, Wyoming. *J. Volcano Geoth. Res.* **188**, 225–236 (2009).

46. Smedes, H. W. & Prostka, H. J. Stratigraphic framework of the Absaroka volcanic supergroup in the Yellowstone National Park region. U.S. Geol. Surv. Report No. 2330–7102, (1972).

47. Fecteau, K. M. et al. Cyanobacteria and algae meet at the limits of their habitat ranges in moderately acidic hot springs. *J. Geophys. Res. Biogeosci.* **127**, e2021JG006446 (2022).

48. Kharaka, Y. K., Thordsden, J. J. & White, L. D. Isotope and chemical compositions of meteoric and thermal waters and snow from the greater Yellowstone National Park region. U.S. Geol. Surv. Open-File Report-2-194 (2002).

49. Kaasalainen, H. & Stefansson, A. The chemistry of trace elements in surface geothermal waters and steam, Iceland. *Chem. Geol.* **330**, 60–85 (2012).

50. Stefánsson, A. et al. GeoFluids database 2016: chemical composition of Icelandic fluids and gases. *Sci. Inst. Report RH-10-2016* (2016).

51. Berg, J. S. et al. How low can they go? Aerobic respiration by microorganisms under apparent anoxia. *FEMS Microbiol. Rev.* **46**, fuac006 (2022).

52. McCleskey, R. B. et al. The source, fate, and transport of arsenic in the Yellowstone hydrothermal system-an overview. *J. Volcanol. Geoth. Res.* **432**, 107709 (2022).

53. Stauffer, R. E. & Thompson, J. M. Arsenic and antimony in geothermal waters of Yellowstone National Park, Wyoming, USA. *Geochim. Cosmochim. Acta* **48**, 2547–2561 (1984).

54. Konstantinidis, K. T. & Tiedje, J. M. Genomic insights that advance the species definition for prokaryotes. *Proc. Natl Acad. Sci. USA* **102**, 2567–2572, (2005).

55. Royo-Llonch, M. et al. Compendium of 530 metagenome-assembled bacterial and archaeal genomes from the polar Arctic Ocean. *Nat. Microbiol.* **6**, 1561–1574 (2021).

56. Alneberg, J. et al. Ecosystem-wide metagenomic binning enables prediction of ecological niches from genomes. *Commun. Biol.* **3**, 119 (2020).

57. Zhou, Z., St. John, E., Anantharaman, K. & Reysenbach, A.-L. Global patterns of diversity and metabolism of microbial communities in deep-sea hydrothermal vent deposits. *Microbiome* **10**, 241 (2022).

58. Inskeep, W. P. et al. The YNP Metagenome Project: environmental parameters responsible for microbial distribution in the Yellowstone Geothermal Ecosystem. *Front. Microbiol.* **4**, 67 (2013).

59. Sharp, C. E. et al. Humboldt's spa: microbial diversity is controlled by temperature in geothermal environments. *ISME J.* **8**, 1166–1174 (2014).

60. Miller, S. R., Strong, A. L., Jones, K. L. & Ungerer, M. C. Bar-coded pyrosequencing reveals shared bacterial community properties along the temperature gradients of two alkaline hot springs in Yellowstone National Park. *Appl. Environ. Microbiol.* **75**, 4565–4572 (2009).

61. Colman, D. R. et al. Tectonic and geologic setting influence hot spring microbiology. *Environ. Microbiol.* **25**, 2481–2497 (2023).

62. Reysenbach, A.-L. et al. Complex subsurface hydrothermal fluid mixing at a submarine arc volcano supports distinct and highly diverse microbial communities. *Proc. Natl Acad. Sci. USA* **117**, 32627–32638 (2020).

63. Colman, D. R. et al. Ecological differentiation in planktonic and sediment-associated chemotrophic microbial populations in Yellowstone Hot Springs. *FEMS Microbiol. Ecol.* **92**, 9 (2016).

64. Hou, W. et al. A comprehensive census of microbial diversity in hot springs of Tengchong, Yunnan Province China using 16S rRNA gene pyrosequencing. *PLoS One* **8**, e53350 (2013).

65. Moreras-Marti, A. et al. Volcanic controls on the microbial habitability of Mars-analogue hydrothermal environments. *Geobiology* **19**, 489–509 (2021).

66. Boyd, E. S., Hamilton, T. L., Wang, J., He, L. & Zhang, C. L. The role of tetraether lipid composition in the adaptation of thermophilic archaea to acidity. *Front. Microbiol.* **4**, 62 (2013).

67. Colman, D. R., Lindsay, M. R., Amenabar, M. J. & Boyd, E. S. The intersection of geology, geochemistry, and microbiology in continental hydrothermal systems. *Astrobiology* **19**, 1505–1522 (2019).

68. Boyd, E. S., Hamilton, T. L., Spear, J. R., Lavin, M. & Peters, J. W. [FeFe]-hydrogenase in Yellowstone National Park: evidence for dispersal limitation and phylogenetic niche conservatism. *ISME J.* **4**, 1485–1495 (2010).

69. Alsop, E. B., Boyd, E. S. & Raymond, J. Merging metagenomics and geochemistry reveals environmental controls on biological diversity and evolution. *BMC Ecol.* **14**, 16 (2014).

70. Payne, D. et al. Geologic legacy spanning >90 years explains unique Yellowstone hot spring geochemistry and biodiversity. *Environ. Microbiol.* **21**, 4180–4195 (2019).

71. Müller, W. J. et al. Whole genome comparison of *Thermus* sp. NMX2. A1 reveals principal carbon metabolism differences with closest relation Thermus scotoductus SA-01. *G3 Genes Genomes Genet.* **6**, 2791–2797 (2016).

72. Balows, A., Trüper, H. G., Dworkin, M., Harder, W. & Schleifer, K.-H. *The prokaryotes: a handbook on the biology of bacteria: ecophysiology, isolation, identification, applications*. Vol. 2 (Springer, 1992).

73. Skirnisdottir, S., Hreggvidsson, G. O., Holst, O. & Kristjansson, J. K. Isolation and characterization of a mixotrophic sulfur-oxidizing *Thermus scotoductus*. *Extremophiles* **5**, 45–51 (2001).

74. Counts, J. A., Willard, D. J. & Kelly, R. M. Life in hot acid: a genome-based reassessment of the archaeal order sulfolobales. *Environ. Microbiol.* **23**, 3568–3584 (2020).

75. Fuchs, G. Alternative pathways of carbon dioxide fixation: insights into the early evolution of life? *Annu Rev. Microbiol.* **65**, 631–658 (2011).

76. Berghuis, B. A. et al. Hydrogenotrophic methanogenesis in archaeal phylum Verstraetearchaeota reveals the shared ancestry of all methanogens. *Proc. Natl Acad. Sci. USA* **116**, 5037–5044 (2019).

77. Ragsdale, S. W. Enzymology of the wood-Ljungdahl pathway of acetogenesis. *Ann. N. Y. Acad. Sci.* **1125**, 129–136, (2008).

78. Windman, T., Zolotova, N., Schwandner, F. & Shock, E. L. Formate as an energy source for microbial metabolism in chemosynthetic zones of hydrothermal ecosystems. *Astrobiology* **7**, 873–890 (2007).

79. Urschel, M. R., Kubo, M. D., Hoehler, T. M., Peters, J. W. & Boyd, E. S. Carbon source preference in chemosynthetic hot spring communities. *Appl. Environ. Microbiol.* **81**, 3834–3847 (2015).

80. Nye, J. J., Shock, E. L. & Hartnett, H. E. A novel PARAFAC model for continental hot springs reveals unique dissolved organic carbon compositions. *Org. Geochem.* **141**, 103964 (2020).

81. Borrel, G. et al. Wide diversity of methane and short-chain alkane metabolisms in uncultured archaea. *Nat. Microbiol.* **4**, 603–613 (2019).

82. Wang, Y., Wegener, G., Hou, J., Wang, F. & Xiao, X. Expanding anaerobic alkane metabolism in the domain of archaea. *Nat. Microbiol.* **4**, 595–602 (2019).

83. McKay, L. J. et al. Co-occurring genomic capacity for anaerobic methane and dissimilatory sulfur metabolisms discovered in the Korarchaeota. *Nat. Microbiol.* **4**, 614–622 (2019).

84. Lynes, M. M., Jay, Z. J., Kohtz, A. J. & Hatzenpichler, R. Methylotrophic methanogenesis in the Archaeoglobi revealed by cultivation of Ca. Methanoglobus hypatiae from a Yellowstone hot spring. *ISME J.* **18**, wrae026 (2024).

85. Vanwonterghem, I. et al. Methylotrophic methanogenesis discovered in the archaeal phylum Verstraetearchaeota. *Nat. Microbiol.* **1**, 16170 (2016).

86. Semrau, J. D., DiSpirito, A. A. & Yoon, S. Methanotrophs and copper. *FEMS Microbiol. Rev.* **34**, 496–531 (2010).

87. Bergfeld, D., Hunt, A. G., Shanks, W., & Evans, W. *Gas and isotope chemistry of thermal features in Yellowstone National Park, Wyoming.* (US Department of the Interior, US Geological Survey, 2014).

88. Zinder, S. & Brock, T. D. Sulfur dioxide in geothermal waters and gases. *Geochim Cosmochim. Ac* **41**, 73–79 (1977).

89. Neukirchen, S., Pereira, I. A. C. & Sousa, F. L. Stepwise pathway for early evolutionary assembly of dissimilatory sulfite and sulfate reduction. *ISME J.* **17**, 1680–1692 (2023).

90. de la Torre, J. R., Walker, C. B., Ingalls, A. E., Konneke, M. & Stahl, D. A. Cultivation of a thermophilic ammonia oxidizing archaeon synthesizing crenarchaeol. *Environ. Microbiol.* **10**, 810–818, (2008).

91. Holloway, J. M., Nordstrom, D. K., Böhlke, J., McCleskey, R. B. & Ball, J. W. Ammonium in thermal waters of Yellowstone National Park: processes affecting speciation and isotope fractionation. *Geochim. Cosmochim. Acta* **75**, 4611–4636 (2011).

92. Hamilton, T. L. et al. Competition for ammonia influences the structure of chemotrophic communities in geothermal springs. *Appl. Environ. Microbiol.* **80**, 653–661 (2014).

93. Romano, C. et al. Comparative genomic analysis of phylogenetically closely related *Hydrogenobaculum* sp. isolates from Yellowstone National Park. *Appl. Environ. Microbiol.* **79**, 2932–2943 (2013).

94. Amend, J. P. & Shock, E. L. Energetics of overall metabolic reactions of thermophilic and hyperthermophilic archaea and bacteria. *FEMS Microbiol. Rev.* **25**, 175–243 (2001).

95. Cozen, A. E. et al. Transcriptional map of respiratory versatility in the hyperthermophilic crenarchaeon Pyrobaculum aerophilum. *J. Bacteriol.* **191**, 782–794 (2009).

96. Muramatsu, F. et al. Possible involvement of a tetrathionate reductase homolog in dissimilatory arsenate reduction by Anaeromyxobacter sp. Strain PSR-1. *Appl. Environ. Microbiol.* **86**, e00829-20 (2020).

97. Garber, A. I. et al. FeGenie: a comprehensive tool for the identification of iron genes and iron gene neighborhoods in genome and metagenome assemblies. *Front. Microbiol.* **11**, 37 (2020).

98. Amenabar, M. J. & Boyd, E. S. Mechanisms of mineral substrate acquisition in a thermoacidophile. *Appl. Environ. Microbiol.* **84**, e00334–00318 (2018).

99. Dunham, E. C., Dore, J. E., Skidmore, M. L., Roden, E. E. & Boyd, E. S. Lithogenic hydrogen supports microbial primary production in subglacial and proglacial environments. *Proc. Nat. Acad. Sci. USA* **118**, e2007051117 (2021).

100. Zavarzina, D., Gavrilov, S. & Zhilina, T. Direct Fe (III) reduction from synthetic ferrihydrite by haloalkaliphilic lithotrophic sulfidogens. *Microbiology* **87**, 164–172 (2018).

101. Liebensteiner, M. G., Tsesmetzis, N., Stams, A. J. & Lomans, B. P. Microbial redox processes in deep subsurface environments and the potential application of (per) chlorate in oil reservoirs. *Front. Microbiol.* **5**, 428 (2014).

102. Barnum, T. P. & Coates, J. D. Chlorine redox chemistry is widespread in microbiology. *ISME J.* **17**, 70–83 (2023).

103. Van Ginkel, C., Rikken, G., Kroon, A. & Kengen, S. Purification and characterization of chlorite dismutase: a novel oxygen-generating enzyme. *Arch. Microbiol.* **166**, 321–326, (1996).

104. Ruff, S. E. et al. Hydrogen and dark oxygen drive microbial productivity in diverse groundwater ecosystems. *Nat. Commun.* **14**, 3194 (2023).

105. Martinez-Gutierrez, C. A. & Aylward, F. O. Phylogenetic signal, congruence, and uncertainty across bacteria and archaea. *Mol. Biol. Evol.* **38**, 5514–5527 (2021).

106. Coleman, G. A. et al. A rooted phylogeny resolves early bacterial evolution. *Science* **372**, eabe0511 (2021).

107. Blank, C. E. Not so old archaea–the antiquity of biogeochemical processes in the archaeal domain of life. *Geobiology* **7**, 495–514 (2009).

108. Ward, L. et al. Microbial community dynamics in Inferno Crater Lake, a thermally fluctuating geothermal spring. *ISME J.* **11**, 1158–1167 (2017).

109. Canfield, D. E. & Teske, A. Late Proterozoic rise in atmospheric oxygen concentration inferred from phylogenetic and sulphur-isotope studies. *Nature* **382**, 127–132, (1996).

110. Ren, M. et al. Phylogenomics suggests oxygen availability as a driving force in Thaumarchaeota evolution. *ISME J.* **13**, 2150–2161 (2019).

111. Gibson, M. L. & Hinman, N. W. Mixing of hydrothermal water and groundwater near hot springs, Yellowstone National Park (USA): hydrology and geochemistry. *Hydrogeol. J.* **21**, 919–933 (2013).

112. Mei, R., Kaneko, M., Imachi, H. & Nobu, M. K. The origin and evolution of methanogenesis and Archaea are intertwined. *PNAS Nexus* **2**, 1–10 (2023).

113. Martin, W., Baross, J., Kelley, D. & Russell, M. J. Hydrothermal vents and the origin of life. *Nat. Rev. Microbiol* **6**, 805–814 (2008).

114. Nitschke, W. & Russell, M. J. Beating the acetyl coenzyme A-pathway to the origin of life. *Philos. Trans. R. Soc. Lond. B Biol. Sci.* **368**, 20120258 (2013).

115. Russell, M. J. & Martin, W. The rocky roots of the acetyl-CoA pathway. *Trends Biochem Sci.* **29**, 358–363, (2004).

116. Inskeep, W. P. et al. Metagenomes from high-temperature chemotrophic systems reveal geochemical controls on microbial community structure and function. *PLoS One* **5**, e9773 (2010).

117. Mulkidjanian, A. Y., Bychkov, A. Y., Dibrova, D. V., Galperin, M. Y. & Koonin, E. V. Origin of first cells at terrestrial, anoxic geothermal fields. *Proc. Natl Acad. Sci. USA* **109**, E821–E830 (2012).

118. Van Kranendonk, M. J. et al. Elements for the origin of life on land: a deep-time perspective from the Pilbara Craton of Western Australia. *Astrobiology* **21**, 39–59 (2021).

119. Upin, H. E., Newell, D. L., Colman, D. R. & Boyd, E. S. Tectonic settings influence the geochemical and microbial diversity of Peru hot springs. *Commun. Earth Environ.* **4**, 112 (2023).

120. Fullerton, K. M. et al. Effect of tectonic processes on biosphere–geosphere feedbacks across a convergent margin. *Nat. Geosci.* **14**, 301–306 (2021).

121. Dahlquist-Selking, G. R., Helfrich, P., Timmer, J. & Cox, A. D. Mudpot geochemistry reveals subsurface geologic activity. *ACS Earth Space Chem.* **7**, 2458–2474 (2023).

122. Lindsay, M. R. et al. Subsurface processes influence oxidant availability and chemoautotrophic hydrogen metabolism in Yellowstone hot springs. *Geobiology* **16**, 674–692 (2018).

123. Spear, J. R., Walker, J. J., McCollom, T. M. & Pace, N. R. Hydrogen and bioenergetics in the Yellowstone geothermal ecosystem. *Proc. Natl Acad. Sci. USA* **102**, 2555–2560 (2005).

124. Martin, M. Cutadapt removes adapter sequences from high-throughput sequencing reads. *EMBnet. J.* **17**, 3 (2011).

125. Nurk, S., Meleshko, D., Korobeynikov, A. & Pevzner, P. A. metaSPAdes: a new versatile metagenomic assembler. *Genome Res.* **27**, 824–834 (2017).

126. Uritskiy, G. V., DiRuggiero, J. & Taylor, J. MetaWRAP-a flexible pipeline for genome-resolved metagenomic data analysis. *Microbiome* **6**, 158 (2018).

127. Li, H. & Durbin, R. Fast and accurate long-read alignment with Burrows-Wheeler transform. *Bioinformatics* **26**, 589–595 (2010).

128. Kang, D. D. et al. MetaBAT 2: an adaptive binning algorithm for robust and efficient genome reconstruction from metagenome assemblies. *PeerJ* **7**, e7359 (2019).

129. Wu, Y. W. et al. An automated binning method to recover individual genomes from metagenomes using an expectation-maximization algorithm. *Microbiome* **2**, 26 (2014).

130. Alneberg, J. et al. Binning metagenomic contigs by coverage and composition. *Nat. Methods* **11**, 1144–1146 (2014).

131. Seemann, T. Prokka: rapid prokaryotic genome annotation. *Bioinformatics* **30**, 2068–2069 (2014).

132. Hyatt, D. et al. Prodigal: prokaryotic gene recognition and translation initiation site identification. *BMC Bioinform.* **11**, 119 (2010).

133. Parks, D. H. et al. GTDB: an ongoing census of bacterial and archaeal diversity through a phylogenetically consistent, rank normalized and complete genome-based taxonomy. *Nucleic Acids Res.* **50**, D785–D794 (2022).

134. Sheik, C. S. et al. Identification and removal of contaminant sequences from ribosomal gene databases: Lessons from the census of deep life. *Front. Microbiol.* **9**, 840 (2018).

135. Woodcroft, B. J. et al. SingleM and Sandpiper: robust microbial taxonomic profiles from metagenomic data. *bioRxiv*, 2024.2001.2030.578060 (2024).

136. Jain, C., Rodriguez, R. L., Phillippy, A. M., Konstantinidis, K. T. & Aluru, S. High throughput ANI analysis of 90K prokaryotic genomes reveals clear species boundaries. *Nat. Commun.* **9**, 5114 (2018).

137. Schloss, P. D. et al. Introducing Mothur: Open-source, platform-independent, community-supported software for describing and comparing microbial communities. *Appl. Environ. Microbiol.* **75**, 7537–7541 (2009).

138. Rodriguez, R. L., Gunturu, S., Tiedje, J. M., Cole, J. R. & Konstantinidis, K. T. Nonpareil 3: fast estimation of metagenomic coverage and sequence diversity. *mSystems* **3**, e00039-18 (2018).

139. vegan: Community Ecology Package v. R package version 2.4 (2017).

140. R: A language and environment for statistical computing v. 3.1.0. (R Foundation for Statistical Computing, Vienna, Austria, 2017).

141. Smoot, M. E., Ono, K., Ruscheinski, J., Wang, P. L. & Ideker, T. Cytoscape 2.8: new features for data integration and network visualization. *Bioinformatics* **27**, 431–432 (2011).

142. Kanehisa, M., Furumichi, M., Tanabe, M., Sato, Y. & Morishima, K. KEGG: new perspectives on genomes, pathways, diseases and drugs. *Nucleic Acids Res.* **45**, D353–D361 (2017).

143. Zhou, Z. et al. METABOLIC: high-throughput profiling of microbial genomes for functional traits, metabolism, biogeochemistry, and community-scale functional networks. *Microbiome* **10**, 33 (2022).

144. Jay, Z. J. et al. Pyrobaculum yellowstonensis strain WP30 respires on elemental sulfur and/or arsenate in circumneutral sulfidic geothermal sediments of Yellowstone National Park. *Appl Environ. Microbiol.* **81**, 5907–5916 (2015).

145. Poudel, S. et al. Origin and evolution of flavin-based electron bifurcating enzymes. *Front. Microbiol.* **9**, 1762 (2018).

146. Schut, G. J., Boyd, E. S., Peters, J. W. & Adams, M. W. The modular respiratory complexes involved in hydrogen and sulfur metabolism by heterotrophic hyperthermophilic archaea and their evolutionary implications. *FEMS Microbiol. Rev.* **37**, 182–203 (2013).

147. Søndergaard, D., Pedersen, C. N. & Greening, C. HydDB: a web tool for hydrogenase classification and analysis. *Sci. Rep.* **6**, 34212 (2016).

148. Koch, T. & Dahl, C. A novel bacterial sulfur oxidation pathway provides a new link between the cycles of organic and inorganic sulfur compounds. *ISME J.* **12**, 2479–2491 (2018).

149. Mardanov, A. V. et al. The genome sequence of the crenarchaeon *Acidilobus saccharovorans* supports a new order, Acidilobales, and suggests an important ecological role in terrestrial acidic hot springs. *Appl. Environ. Microbiol.* **76**, 5652–5657 (2010).

150. Laska, S., Lottspeich, F. & Kletzin, A. Membrane-bound hydrogenase and sulfur reductase of the hyperthermophilic and acidophilic archaeon Acidianus ambivalens. *Microbiology* **149**, 2357–2371 (2003).

151. Sunagawa, S. et al. Metagenomic species profiling using universal phylogenetic marker genes. *Nat. Methods* **10**, 1196–1199 (2013).

152. Sievers, F. et al. Fast, scalable generation of high-quality protein multiple sequence alignments using Clustal Omega. *Mol. Syst. Biol.* **7**, 539 (2011).

153. Capella-Gutierrez, S., Silla-Martinez, J. M. & Gabaldon, T. trimAl: a tool for automated alignment trimming in large-scale phylogenetic analyses. *Bioinformatics* **25**, 1972–1973, (2009).

154. Minh, B. Q. et al. IQ-TREE 2: new models and efficient methods for phylogenetic inference in the genomic era. *Mol. Biol. Evol.* **37**, 1530–1534 (2020).

Acknowledgements

Author contributions

D.R.C. and E.S.B. designed the study and prepared the manuscript. D.R.C. conducted the analyses and L.M.K. contributed to genomic data generation. E.A.P., E.A.B., B.S.C., A.C., and D.R.C. generated and analyzed geochemical data. A.S. aided in figure preparation and map construction. D.R.C., E.S.B., L.M.K., E.A.P., E.A.B., B.S.C., A.C., and D.R.C. contributed to field sampling. All authors contributed to manuscript preparation.

Competing interests

The authors declare no competing interests.

Additional information